Physics – Uspekhi **64** (5) 495 – 514 (2021)

INSTRUMENTS AND METHODS OF INVESTIGATION PACS numbers: **07.60.–j**, **07.85.–m**, 07.85.Fv, 07.85.Nc, **07.87.+v**, **42.79.–e**

Soft X-ray spectrometers based on aperiodic reflection gratings and their application

E N Ragozin, E A Vishnyakov, A O Kolesnikov, A S Pirozhkov, A N Shatokhin

DOI: https://doi.org/10.3367/UFNe.2020.06.038799

Contents

1. **Introduction. Brief historical background** **495**
2. **Equations describing the focusing properties of VLS gratings** **496**
3. **Concave VLS grating and its application. Flat-field grazing-incidence spectrometer. Harada spectrograph** **497**
4. **Plane VLS grating and its application. High/ultrahigh-resolution grazing-incidence scanning spectrometer/monochromator** **500**
5. **Spectrometers for recording resonant inelastic X-ray scattering** **502**
6. **VLS gratings for the 'tender' X-ray domain** **503**
7. **Application of VLS spectrometers in vacuum ultraviolet astronomy** **505**
8. **X-ray spectrometer based on a reflection zone plate** **506**
9. **Domestic soft X-ray VLS spectrometers** **507**
   9.1 Imaging (stigmatic) spectrograph for a wavelength range of 12 – 30 nm; 9.2 Scanning spectrometer/monochromator for a wavelength range of ~ 5 – 33 nm; 9.3 Flat-field spectrometer for a wavelength range of 5 – 27.5 nm
10. **VLS-grating fabrication technologies** **511**
11. **Conclusions** **513**
    References **513**

Abstract. **This paper is concerned with the history, properties, development, application, and prospects of soft X-ray (2 – 300 Å) VLS spectrometers, i.e., spectrometers with reflection diffraction gratings whose spacing varies monotonically across the aperture according to a prescribed law (so-called Varied Line-Space (VLS) gratings). An important feature of grazing-incidence VLS spectrometers is that the spectrum is formed on a nearly flat surface perpendicular (or slightly inclined) to the diffracted beams, making them perfectly compatible with modern CCD detectors. VLS spectrometers are employed for the spectroscopy of laboratory and astrophysical plasmas, including the diagnostics of relativistic laser-produced plasmas, for measuring the linewidth of an X-ray laser, for recording the high-order harmonics of laser radiation, and for recording the emission of fast electric discharges and other laboratory X-ray sources. Instruments with VLS gratings are employed to advantage in reflectometry/metrology, X-ray fluorescence analysis, and microscopy with the use of synchrotron, free-electron laser, and laser-produced plasma radiation, as well as in SXR emission spectroscopy, combined with an electron microscope (SXES). Recent years have seen the active development of VLS spectrometers dedicated to the investigation of the electronic structure of different materials and molecules by resonant inelastic X-ray scattering (RIXS) spectroscopy with synchrotron radiation. Among recent trends is the development of VLS gratings with a multilayer reflective coating and extension of the operating spectral range towards 'tender' X-rays ($\hbar\omega \sim 1.5 - 6$ keV), some projects aiming to achieve a resolving power $\lambda/\delta\lambda \sim 10^5$ in the region $\hbar\omega \sim 1$ keV.**

Keywords: soft X-ray radiation, aperiodic reflection diffraction grating (VLS grating), flat-field spectrometer, scanning spectrometer/monochromator, stigmatic (imaging) spectrometer

E N Ragozin [1,*], **E A Vishnyakov** [1], **A O Kolesnikov** [1,2], **A S Pirozhkov** [3], **A N Shatokhin** [1]
[1] Lebedev Physical Institute, Russian Academy of Sciences, Leninskii prosp. 53, 119991 Moscow, Russian Federation
[2] Moscow Institute of Physics and Technology (National Research University), Institutskii per. 9, 141701 Dolgoprudny, Moscow region, Russian Federation
[3] Kansai Photon Science Institute (KPSI), National Institutes for Quantum and Radiological Science and Technology (QST), 8-1-7 Umemidai, Kizugawa, Kyoto, 619-0215 Japan
E-mail: [*] enragozin@gmail.com

Received 25 April 2020, revised 27 June 2020
Uspekhi Fizicheskikh Nauk **191** (5) 522 – 542 (2021)
Translated by E N Ragozin

1. Introduction. Brief historical background

In 1882, H A Rowland conceived the idea to combine the dispersive properties of a plane diffraction grating (DG) with the focusing action of a concave mirror [1]. He found that concave gratings possessed a remarkable property: when a concave grating is placed tangentially to a circle of radius equal to half the grating radius, the spectrum of a point source placed on this circle will be focused on this circle. This circle was called the Rowland circle, and this source–grating configuration was referred to as the Rowland mount and became the basis for the majority of vacuum

spectrographs[1] [1, 2]. With the use of his ruling engine, Rowland was able to rule excellent gratings[2] with a line density up to $\sim 1690\ \mathrm{mm}^{-1}$. Transition to spectrographs with grazing radiation incidence on the grating [4] enabled spectroscopists to master the soft X-ray (SXR) (2 – 300 Å) spectral range. The problems of spectroscopy of the vacuum spectral region are addressed in B Edlen's review published in the journal *Physics–Uspekhi* in 1966 [5]. For many decades — nearly a century — the efforts of grating manufacturers were aimed at maximizing the equidistance of the grooves, because the equidistance of the grooves of classical gratings signified a high resolving power and was associated with their quality.

In 1893, M Cornu determined that a uniform variation of the spacing of a reflective diffraction grating across its aperture results in a change to the curvature of the wavefronts of diffracted beams [6]. He found that a plane grating with the requisite systematic variation of the spacing, when placed in a collimated incident beam, would focus the diffracted beam. In the 1970s–1980s, the idea of employing the focusing properties of aperiodic gratings was approached by T Harada [7–10], M Hettrick, and J Underwood [11, 12]. Nowadays, gratings with a spacing that varies monotonically across the aperture according to a prescribed law are referred to as varied line-space (VLS) gratings, use being made both of plane and of concave VLS gratings. The scope of their application in optics and spectroscopy of the SXR spectral domain is quite broad.

At present, VLS gratings enjoy wide use in various problem-oriented spectrometers for the investigation of emission spectra of laser-produced plasma and fast electric discharges and in astrophysics, synchrotron radiation channels, metrology, reflectometry, X-ray fluorescence analysis and microscopy with the use of synchrotrons, free-electron lasers (FELs) and other radiation sources, the analysis of biological samples, etc. An important property of VLS-grating-based spectrometers is that the spectrum is formed on a flat surface, which is perpendicular (or slightly inclined) to the diffracted beams. This makes them compatible with modern solid-state detectors with electrical image readout (in particular, with backside-illuminated array charge-coupled devices (CCDs)) and a plane sensitive surface. Some configurations involving VLS gratings construct stigmatic spectral images in the SXR region.

The advent of VLS gratings, along with multilayer mirrors, free-standing transmission gratings, Fresnel zone-plates, etc., has become a constituent of the renaissance of X-ray optics [13].

In defining the subranges of the vacuum domain of the electromagnetic spectrum, we adhere to the monograph by J Samson [2], who ascribed a wavelength range of 2 – 300 Å to SXR radiation. In recent years, a narrow wavelength range (approximately 2 – 8 Å, or 6–1.5 keV), which is adjacent to hard X-rays, is also referred to as the 'tender' X-ray range.

The aim of our review is to show the new potential furnished by plane and concave VLS gratings in comparison with classical gratings with equidistant grooves, to provide examples of the use of VLS gratings in modern experiments and SXR metrology, to emphasize the trends in VLS spectrometry, and to give a brief outline of the work along these lines commenced in the Spectroscopy Department of the Lebedev Physical Institute (LPI) of the Russian Academy of Sciences.

2. Equations describing the focusing properties of VLS gratings

The focusing properties and aberrations of a VLS grating (plane, concave) may be determined using the Fermat principle, which calls for the calculation of the optical path function $F(\mathrm{P})$. We restrict ourselves to a consideration of spherical concave and plane VLS gratings with a varied spacing and straight grooves, which arise from the intersection of the grating surface with the planes parallel to the xz plane (Fig. 1). For simplicity, we ignore the shape of DG grooves and assume them to be lines of zero width. The real groove shape would be significant in the determination of intensity distribution in the spectrum. Let us place the origin of the rectangular coordinate system at the center of the concave DG; point $\mathrm{C}(R, 0, 0)$ is the center of the sphere on which the DG is made; the x-axis is directed along the normal to the grating, and the y-axis is perpendicular to the grooves. The xy plane is called the principal plane. $\mathrm{A}(x, y, z)$, $\mathrm{B}(x', y', z')$, and $\mathrm{P}(u, w, l)$ denote, respectively, a point source (for example, the illuminated point of the entrance slit), its spectral image, and any point of a groove on the surface of the DG. The grooves of the classical DG are equidistant along the span of the grating (in the y direction); the variable w assumes only discrete values, so that the ratio w/d takes on a number of integer values, where $d = p^{-1}$ is the DG constant (period), and p is the constant groove frequency. In the case of a VLS grating, the groove frequency is conveniently represented as a polynomial,

$$p(w) = p_0 + p_1 w + p_2 w^2 + p_3 w^3 + \dots , \tag{1}$$

with $\mathrm{d}n/\mathrm{d}w = p(w)$, where $n(w)$ is the groove number.

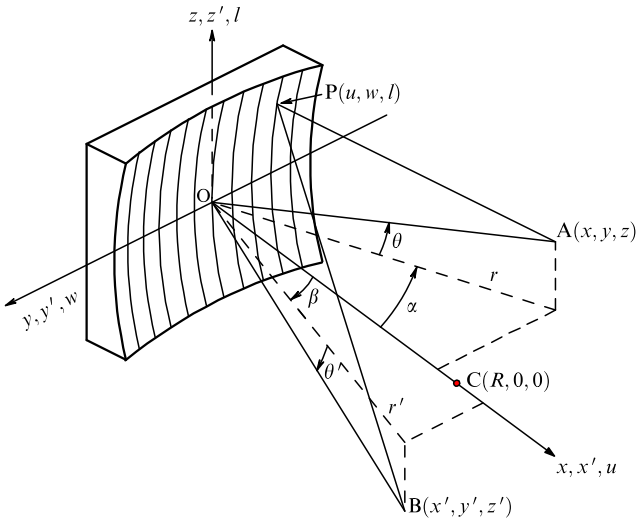

Figure 1. Concave diffraction grating: points A and B — point radiation source and its spectral image produced by the grating; $\mathrm{C}(R, 0, 0)$ is the center of the sphere; O is the grating center; r and r' are lengths of the projections of segments AO and BO on the principal plane xy; α is the incidence angle; β is the diffraction angle. The spacing of the VLS grating varies monotonically across the aperture. In general, a distinction should be made between the distance to the horizontal (spectral) focus r'_{h} and the vertical focus r'_{v}.

[1] The terms 'spectrograph' and 'spectrometer' are used as synonyms.

[2] Rowland stated that his ruling engine had the capacity to rule gratings with a line density at least two or three times higher than that. In doing this, he believed that such gratings would be useless. The discovery of vacuum ultraviolet (VUV) radiation was reported by V Schumann eleven years later [3]. Modern reflective and transmission gratings used in the vacuum spectral domain range up to $\sim 10^4\ \mathrm{mm}^{-1}$ in line frequency.

Point B is the spectral image of point A. According to the Fermat principle, point B is located such that function $F(\mathrm{P}) - m\lambda n(w)$ is extremal relative to small displacements of P, specifically, $\partial F/\partial w = m\lambda p(w)$ and $\partial F/\partial l = 0$. If these conditions could be satisfied simultaneously, point B would be a perfect focal point. However, a concave DG does not produce a perfect image. The point of intersection of the beam, which is diffracted at a point $\mathrm{P}(u, w, l)$, with an arbitrary smooth surface passing through point B depends slightly on the coordinates of point P and is at some small distance from point B.

The optical path function is of the form $F = \mathrm{AP} + \mathrm{PB}$. We assume that the source is close to the principal plane and take advantage of the expansion of the sum $\mathrm{AP} + \mathrm{PB}$ borrowed from Ref. [14]. We then apply the Fermat principle to obtain

$$\frac{\partial F}{\partial w} = \left[\left(1 + \frac{z^2}{r^2}\right)^{-1/2} \sin\alpha + \left(1 + \frac{z'^2}{r'^2}\right)^{-1/2} \sin\beta\right] + w\left(\frac{\cos^2\alpha}{r} - \frac{\cos\alpha}{R} + \frac{\cos^2\beta}{r'} - \frac{\cos\beta}{R}\right) + \ldots = m\lambda p(w)\,, \tag{2}$$

$$\frac{\partial F}{\partial l} = -\left[\frac{z}{r}\left(1 + \frac{z^2}{r^2}\right)^{-1/2} + \frac{z'}{r'}\left(1 + \frac{z'^2}{r'^2}\right)^{-1/2}\right] + l\left(\frac{1}{r} - \frac{\cos\alpha}{R} + \frac{1}{r'} - \frac{\cos\beta}{R}\right) - \frac{l}{2}\left[\frac{z^2}{r^2}\left(\frac{3}{r} - \frac{\cos\alpha}{R}\right) + \frac{z'^2}{r'^2}\left(\frac{3}{r'} - \frac{\cos\beta}{R}\right)\right] \ldots = 0\,, \tag{3}$$

where $p(w)$ is given by expression (1). In Eqn (2), we discarded the expansion terms containing nonzero powers of l and powers of w higher than the first, and in Eqn (3), we discarded the expansion terms containing nonzero powers of w and powers l higher than the first. Sequentially equating to zero different terms of expansions (2) and (3), one can obtain the diffraction equations for the central ray (i.e., the ray passing through the point O) and determine the position of the paraxial foci.

The equations that determine the direction of diffraction of the central ray coincide with the expressions for diffraction by a classical DG, since they are obtained in the limit $w \to 0$, $l \to 0$ (we take into account that $(1 + z^2/r^2)^{-1/2} = \cos\theta$):

$$\cos\theta(\sin\alpha + \sin\beta_0) = m\lambda p_0\,, \tag{4}$$

$$\theta = -\theta_0'\,. \tag{5}$$

Here, angle β_0 is called the angle of diffraction of the central ray AO and is equal to the angle between the grating normal OC and the projection of diffracted ray OB on the principal plane, and θ_0' is the angle that the OB beam makes with the principal plane. Equations (4) and (5) describe the direction of diffraction of the central ray, Eqn (4) being called the diffraction grating equation. It also implies that the direction of each ray is defined by the local groove frequency.

Equating to zero the coefficient at w in Eqn (2) gives

$$\frac{\cos^2\alpha}{r} - \frac{\cos\alpha}{R} + \frac{\cos^2\beta}{r_\mathrm{h}'} - \frac{\cos\beta}{R} - m\lambda p_1 = 0\,. \tag{6}$$

This equation describes the location of the horizontal (spectral) focus r_h' of a thin horizontal fan of paraxial rays about AOB. It differs from the corresponding equation for the classical grating in that the term $m\lambda p_1$ appears. The position r_v' of the vertical focus, that is, the focus for the vertical fan of paraxial rays about AOB, is still described by the equation

$$\frac{1}{r} - \frac{\cos\alpha}{R} + \frac{1}{r_\mathrm{v}'} - \frac{\cos\beta}{R} = 0\,, \tag{7}$$

which is obtained if the next (linear in l) term in $\partial F/\partial l = 0$ is equated to zero. The vertical focus very rarely coincides with the horizontal one (astigmatism of the diffraction grating). The only nontrivial solution in which both paraxial foci of a spherical equidistant DG coincide is the Wadsworth mount [2].

For a plane DG ($R \to \infty$), Eqns (6), (7) are of the form

$$\frac{\cos^2\alpha}{r} + \frac{\cos^2\beta}{r_\mathrm{h}'} - m\lambda p_1 = 0\,, \tag{8}$$

$$\frac{1}{r} + \frac{1}{r_\mathrm{v}'} = 0\,. \tag{9}$$

Therefore, the location of the spectral focus depends on the value of the derivative $\mathrm{d}p(w)/\mathrm{d}w = p_1$, which gives the focusing power in nonzero diffraction orders even to a plane diffraction grating. Using the coefficients p_2 and p_3 from Eqn (1), the meridional coma and spherical aberration are minimized, respectively [15].

To improve the DG efficiency in the region $\lambda < 300$ Å, recourse is made to a grazing incidence of radiation on the grating. Then, it is convenient to use the grazing angles of incidence $\varphi = \pi/2 - \alpha$ and diffraction $\psi = \pi/2 + \beta$, which are measured from the tangent to the DG at its center. In this case, Eqns (4), (6), and (7) take the form

$$\cos\theta(\cos\varphi - \cos\psi) = m\lambda p_0\,, \tag{10}$$

$$\frac{\sin^2\varphi}{r} - \frac{\sin\varphi}{R} + \frac{\sin^2\psi}{r_\mathrm{h}'} - \frac{\sin\psi}{R} = m\lambda p_1\,, \tag{11}$$

$$\frac{1}{r} - \frac{\sin\varphi}{R} + \frac{1}{r_\mathrm{v}'} - \frac{\sin\psi}{R} = 0\,. \tag{12}$$

In this case, the diffraction angles will also be grazing, and expression (12) gives an imaginary vertical focus $r_\mathrm{v}' < 0$, unless the source is a long distance away from the grating or, moreover, is not imaginary (is not a converging beam). This signifies that the diffracted beams will diverge in the vertical direction and the spectral images will be astigmatic.

3. Concave VLS grating and its application. Flat-field grazing-incidence spectrometer. Harada spectrograph

In the Rowland mount, the diffracted radiation is incident on the focal surface at a small grazing angle equal to the diffraction angle $\psi(\lambda)$. This makes the classical Rowland mount incompatible with modern CCD array detectors: installing the detector perpendicular to the diffracted rays leads to a loss of spectral resolution or a significant narrowing of the operating spectral range, and installing it tangentially to the Rowland circle leads to signal attenuation due to an increase in absorption in the dead layer of the detector and reflection from its surface.

To efficiently use the concave grating in combination with the CCD detector, the focal curve should be changed so that a rectilinear section appears on it, oriented almost normally to the diffracting beams. Figure 2 shows a family of focal curves

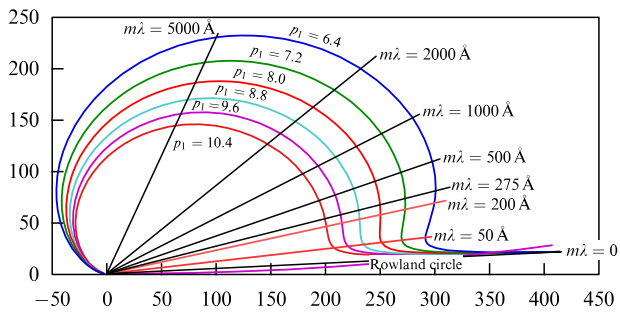

Figure 2. Family of spectral (horizontal) focal curves corresponding to different values of parameter p_1 (a half-meter spectrograph of the Harada class). The axial scales are marked in mm. The origin coincides with the VLS-grating center ($R = 6$ m, $p_0 = 1200$ mm^{-1}, $\varphi = 3°$, $r = 252$ mm).

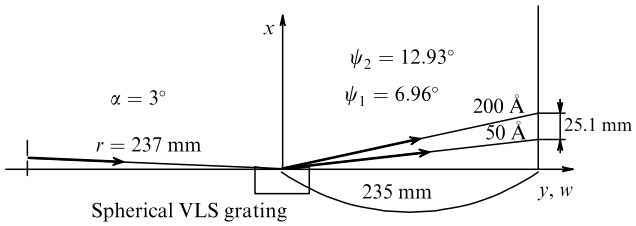

Figure 3. Harada spectrograph [9]. Spherical VLS grating ($R = 5649$ mm) with $p_0 = 1200$ mm^{-1} forms a plane portion of the focal curve in a wavelength range of 50–200 Å in the 7°–13° range of angles of radiation incidence on the detector. The grating spacing varies from 0.99 to 0.69 μm across the 50-mm aperture.

corresponding to different values of parameter p_1 for a VLS grating with $R = 6$ m and $p_0 = 1200$ mm^{-1} for $\varphi = 3°$ and an entrance slit–grating distance of 252 mm [16]. Inclined straight lines indicate the directions of diffraction of radiation with different wavelengths. One can see for $p_1 = 8.0$ mm^{-2} that the portion of the focal curve between the rays with $m\lambda \approx 50$ and 275 Å is reasonably well approximated by a straight line segment perpendicular to the horizontal axis coinciding with the tangent to the center of the grating (the origin). The flat sensitive surface of the detector should be aligned with this segment.

This line was pioneered by T Harada (Hitachi, Japan), who designed a half-meter flat field spectrograph for a range of 50–200 Å based on a VLS grating (Fig. 3) and implemented a programmable mechanical ruling engine, which enabled ruling plane and concave VLS gratings with a groove frequency of up to 10,000 mm^{-1} and a minimum spacing increment of 0.2 Å [8, 10]. The Harada half-meter spectrograph was demonstrated in operation when recording the spectra of laser-produced plasma [9], became commercially available, and has enjoyed world-wide use.

The shape of the focal surface of the instrument depends only on the p_1/p_0 coefficient ratio, the grazing-incidence angle φ, the radius of curvature R of the grating, and the distance r of the entrance slit from the grating center. In addition, it is easy to verify that aberrations are compensated for certain values of the ratios p_2/p_0 and p_3/p_0 for a fixed diffraction angle. Therefore, a proportional increase or decrease in all the grating coefficients will not change the image of the spectral line at the same diffraction angle, but will change the wavelength corresponding to it. This means that on calculating a successful geometry of the instrument for any wavelength region, it can be transferred to another wavelength

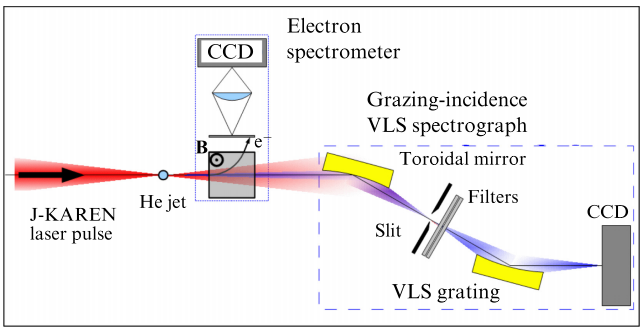

Figure 4. Recording of high-order harmonics generated in the helium plasma produced by the radiation of a multiterawatt femtosecond laser [18]. The harmonics spectrum, which lies in the far-VUV and SXR domain, is recorded with a Harada spectrograph and an additional grazing-incidence toroidal mirror.

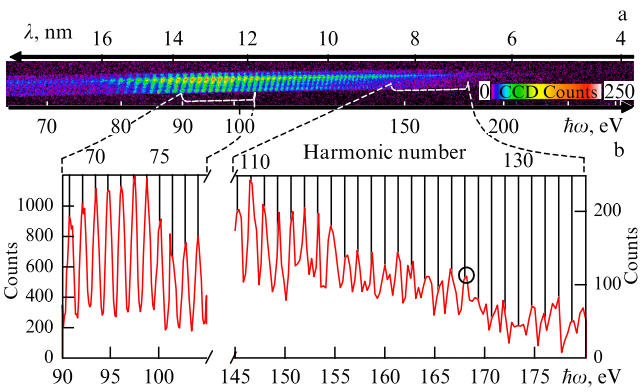

Figure 5. (a) Typical harmonics spectrum generated in a helium plasma, which was produced under multiterawatt femtosecond titanium-sapphire laser irradiation at a laser power $P_0 = 9$ TW and a peak electron density $n_e = 4.7 \times 10^{19}$ cm^{-3} [18]. (b) Lineouts of two selected portions of the spectrum. Vertical lines indicate the positions of harmonics $n_h\omega_f$ of the base frequency $\omega_f = 0.885\omega_0$, where ω_0 is the frequency of laser radiation. The highest number of the clearly discernible harmonic $n_h^* = 126$ (marked with a circle).

region by simple proportional scaling of all the terms of expansion (1) of $p(w)$ (provided that the efficiency of the grating is sufficient for a given φ) [17].

A modern example of using the Harada spectrograph is the recording of high-order harmonics of laser radiation generated in a relativistic helium laser plasma produced under irradiation by a multi-terawatt femtosecond J-KAREN laser (Japan) with a focal intensity of more than 10^{18} W cm^{-2} (Fig. 4) [18, 19]. A grazing incidence toroidal mirror images the SXR radiation source at the input of the Harada spectrograph (horizontal focus), while the vertical focus is onto a detector. In this case, both even and odd harmonics are generated, and their frequencies are multiples of the base frequency ω_f, which is somewhat lower than the carrier frequency of the femtosecond titanium-sapphire laser radiation (Fig. 5). The high quality of the recorded spectra made it possible to formulate the hypothesis that the harmonics were generated by density singularities formed during the multi-flow motion of the plasma. This hypothesis was experimentally borne out in Ref. [20], where images and spectra of coherent point sources were recorded in the spectral range of 12–20 nm. Such sources are a special case of a more general phenomenon called BISER (Burst Intensification by Singularity Emitting Radiation) [20].

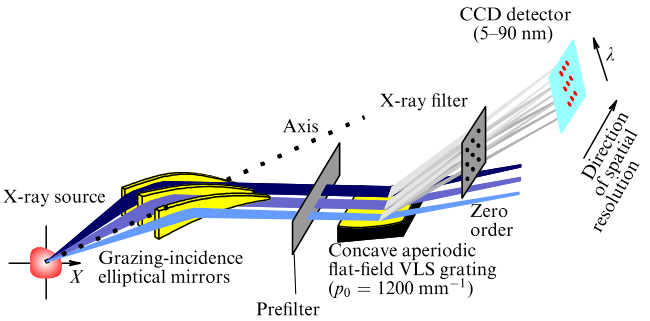

Figure 6. Three-channel slitless flat-field imaging spectrometer with the Harada grating. (Adapted from Ref. [21].)

A slitless version of the VLS spectrometer was also used to record the harmonics. At the Rutherford–Appleton Laboratory (Great Britain), a slitless three-channel flat-field VLS spectrometer was designed for the range of 5–90 nm, one of the purposes of which was to estimate the angular distribution of harmonic radiation [21] (Fig. 6). Three grazing-incidence mirrors, which were given the shape of elliptical cylinders, intercepted the harmonic radiation emanating at angles of 0 ± 13, 46 ± 21, and 108 ± 35 mrad. The mirrors were crossed with respect to the grating and each constructed a one-dimensional image of the X-ray source on the detector, whereas the VLS grating ($R = 5649$ mm, aperture $W = 50 \times 30$ mm, manufactured by Hitachi) constructed its dispersed spectral images focused in the crossed direction. Therefore, the device was a flat-field stigmatic (imaging) spectrometer. Subsequently, a VLS grating with $p_0 = 2400$ mm^{-1} was also used [22].

To record radiation in the region $\lambda < 50$ Å, spectrographs were made based on gold-coated VLS gratings ($R = 15.92$ m) with $p_0 = 2400$ mm^{-1} [22, 23], the researchers having at their disposal both mechanically ruled gratings and gratings made by interference lithography (IL). The slit–grating (237 mm) and grating–detector (235 mm) distances of the VLS-spectrograph setup were the same as in Ref. [9] (see Fig. 3), but the grazing-incidence angle was 1.35°. In Ref. [22], the characteristic K-lines of oxygen (23.6 Å), magnesium (9.89 Å), and silicon (7.13 Å) were recorded at a grazing angle of 1.35° using a VLS grating made using the IL technique, and its efficiency was measured in the range of 8–45 Å. At a wavelength of ~ 10 Å, the grating efficiency was higher than 1.5% in the first diffraction order. It was noted that the efficiency of the grating made by the IL technique in the region $\lambda < 45$ Å was higher than the efficiency of the ruled grating. The operating range of these VLS spectrographs is adjacent to the 'tender' X-ray range. The lines of H- and He-like carbon ions, as well as the resonance lines of O VII and O VIII (19 Å) ions, were recorded when the carbon target was irradiated by 150-ps Nd:YAG-laser pulses with an energy up to 0.25 J [23]. The width of the 1s–2p C VI ion line (33.7 Å) corresponded to a resolving power $\lambda/\delta\lambda = 277$.

A spherical VLS-grating spectrograph combined with an electron microscope is also used in SXR emission spectroscopy (SXES spectroscopy) [24–26]. In this case, the emission is excited by the focused electron beam, making it possible to record spectra with a high spatial resolution. The application of VLS gratings permits a significant improvement in spectral resolution and sensitivity of the instruments in the determination of impurities and chemical bonds. The combination of an electron microscope and an SXR spectrograph is widely used in material science, in the development of energy storage devices (for instance, lithium-ion batteries), etc.

In Ref. [26], a half-meter spectrograph with four replaceable spherical VLS gratings, which spanned a wavelength range almost two orders of magnitude wide, was designed for SXES (Table 1). The operating spectral range begins from the K line of Li (54 eV) and encompassed, in particular, the M lines of Pt: M_α (2050 eV) and M_β (2127 eV). The resolving power of the instrument was measured in experiments with a laser-plasma source of line radiation and was ~ 1000 in the vicinity of an energy of 40 eV and at least 700 near the K line of Li. The K spectrum of metallic lithium excited in an electron microscope was recorded.

SEM-SXES (Scanning Electron Microscope–Soft X-ray Emission Spectrometer) instruments are commercially available [27].

The practical spectral resolution of a grazing-incidence flat-field VLS spectrometer (see Fig. 3) is defined by the linear dispersion and the spatial detector resolution. Numerically, it is approximately equal to the product of the doubled detector pixel size s and the plate scale $\mathrm{d}\lambda/\mathrm{d}x$:

$$\delta\lambda \approx 2s\,\frac{\mathrm{d}\lambda}{\mathrm{d}x}\,, \quad \text{where} \quad \frac{\mathrm{d}\lambda}{\mathrm{d}x} = \frac{\cos^2\psi}{L}\,\frac{\mathrm{d}\lambda}{\mathrm{d}\psi} = \frac{\cos^2\psi\,\sin\psi}{Lmp}\,, \quad (13)$$

and L is the DG–detector distance measured along the y-axis. The factor $\cos^2\psi$ arises from the fact that the radiation is not quite normally incident on the detector and may in fact be

Table 1. Parameters of VLS gratings intended for soft X-ray emission spectroscopy (SXES) [26].

Energy range, eV	50–200	155–350	300–2200	2000–4000
Wavelength range, nm	25–6	8.0–3.5	4.13–0.56	0.62–0.31
Grazing incidence angle, °	4	2.93	1.35	1.35
p_0, mm^{-1}	1200	1200	2400	2400
Radius of curvature, mm	3960	5606	13,800	11,200
Projection of the segment between source and DG center on the y-axis, mm	236.69			
Distance along the y-axis between the DG center and the detector plane, mm	233.50			
Coating	Au	Ni	Au	Mo/C multilayer, 5.2-nm period, 30 periods [26]

ignored. All other factors being the same, the resolving power $\lambda/\delta\lambda$ becomes lower with decreasing wavelength. One can see from Eqn (13) that a high resolving power may be maintained by lengthening the DG–detector distance and raising the grating line frequency, as well as by decreasing s, the last two factors being technologically limited.[3] Another possibility involves decreasing angle ψ by using an external diffraction order ($m < 0$, $\psi < \varphi$). However, due to the angular magnification,

$$\left|\frac{\mathrm{d}\psi}{\mathrm{d}\varphi}\right| = \frac{\sin\varphi}{\sin\psi} > 1\,, \tag{14}$$

the width of the entrance slit has to be decreased, which lowers the illumination in spectral lines and imposes heavy demands on the spectral brightness of the source. This approach was implemented in Hettrick–Underwood class spectrometers with a plane VLS grating (see Section 4 below).

As for increasing the DG–detector distance, this is used in the grazing-incidence flat-field VLS spectrograph ($\varphi \sim 2^\circ$) for a region of $10-50$ Å designed at the Lawrence Livermore National Laboratory (LLNL, USA) [28, 29]. Use was made of a VLS grating with a long radius of curvature ($R = 44.3$ m) and $p_0 = 2400\ \mathrm{mm}^{-1}$. The groove frequency varied across the aperture from 2270 to 2540 mm^{-1}. A strong linear dispersion was achieved due to a much longer grating–detector distance than in Ref. [9]. The total length of the instrument was about 3 m. The spectrometer developed by LLNL was designed to record SXR radiation spectra excited in an electromagnetic trap (EBIT), which produced and retained multiply charged ions [28]. It was noted that the spectrometer provided a higher resolving power in the specified spectral region (600 at $\lambda = 16$ Å and 1200 at $\lambda = 35$ Å) than the existing grating spectrometers, and also complemented short-wavelength crystal spectrographs in terms of spectral range coverage and polarization-independent response. More recently, the VLS spectrometer developed at LLNL for the $10-50$ Å range was used to record spectra excited in the laser plasma of various targets [29]. A cooled CCD array was used as a detector. Presented in Ref. [29] were excellent spectra of the Lyman series of H-and He-like oxygen ions (including dielectronic satellites) excited by laser irradiation of a 3-μm-thick dacron film and a 300-μm-thick aerogel layer with a density of 50 mg cm^{-3}. A spectral resolving power of over 1200 was achieved in a region of $\lambda \sim 19$ Å.

Lengthening the DG–detector distance is also planned in resonant inelastic X-ray scattering spectrometers in order to achieve a resolving power of 10^4-10^5 (see Section 5 below).

4. Plane VLS grating and its application. High/ultrahigh-resolution grazing-incidence scanning spectrometer/monochromator

Another class of SXR instruments in demand are monochromators/spectrometers with a high spectral resolution, a constant deflection angle, an immobile entrance slit, and an immobile exit slit (detector); wavelength tuning is accomplished by the rotation of a plane VLS grating. The idea of this approach was introduced by Hettrick and Underwood [11]. A slit is placed at the output of the instrument in the monochromator mode, and a detector with spatial resolution (e.g., a CCD) is installed in the scanning monochromator mode, in which case, for a fixed angle of grating rotation, good focusing and a high resolution persist in rather broad spectral intervals, whose width depends on specific configuration parameters. For instance, in the scanning spectrometer/monochromator described in Section 9.2, this interval is approximately ± 10 Å. The Hettrick–Underwood scanning spectrometer is a flat-field instrument, whose focal curve is nearly perpendicular to the diffracting rays, making it perfectly compatible with modern CCD detectors. Owing to the specified combination of properties, scanning spectrometers/monochromators with plane VLS gratings have gained wide acceptance and become commercially available [30].

Experimentally, the use of instruments with constant radiation input and output directions, i.e., with a constant deflection angle Ω, and constant distances to the entrance slit and the exit slit (or to the radiation detector) is far preferable to the use of instruments for which wavelength tuning necessitates a significant change in the entire configuration setup. In a configuration with a constant deflection angle, the angle of incidence of the central beam on the grating is related to the wavelength by the expressions

$$\begin{aligned} \varphi &= \frac{\Omega}{2} - \arcsin\frac{m p_0 \lambda}{2\sin(\Omega/2)}\,, \\ m\lambda &= \frac{2\sin(\Omega/2)\sin(\Omega/2-\varphi)}{p_0}\,, \end{aligned} \tag{15}$$

which follow from the diffraction grating equation $\cos\varphi - \cos\psi = m\lambda p_0$ on imposing the condition that the deflection angle be constant: $\varphi + \psi = \Omega$. In oblique — and even more so in grazing — radiation incident on the grating, inside and outside diffraction orders are used differently.[4] As is well known, the special feature of employing an outside diffraction order in the configuration with a constant deflection angle is that moving to shorter wavelengths takes place at smaller grazing angles of incidence on the grating, making it possible to maintain the reflection coefficient at a sufficiently high level.

Let the frequency of the grating grooves vary along the aperture according to the law $p = p_0 + p_1 w$. A grazing-incidence spherical mirror directs a converging beam onto a plane VLS grating, constructing an image (horizontal focus) of the entrance slit behind the grating at a distance r_h from its center (Fig. 7). The horizontal focus of the diffracted radiation is located at a distance r'_h defined by formula (11) for $R = \infty$, where we conveniently assume r_h to be positive:

$$m\lambda p_1 = -\frac{\sin^2\varphi}{r_\mathrm{h}} + \frac{\sin^2\psi}{r'_\mathrm{h}}\,. \tag{16}$$

The condition that distance r'_h be constant can be fulfilled for two wavelengths $\lambda_{1,2}$ for a constant distance to the

[3] In some cases, it is possible to obtain a subpixel resolution. For instance, when recording a stationary process, this may be achieved by shifting the detector by a small fraction of the pixel size and each time recording the spectral line profile, with the subsequent solution to the inverse problem. Another possibility consists of setting the axis of the 2D detector array at a small angle to a vertically uniform spectral line. In either case, the capabilities of the method are limited, as usual, by noise.

[4] By definition, the term *inside diffraction orders* is used in reference to those which are deflected from the zero order to the side of the incident beam, and the term *outside orders*, in reference to those deflected to the other side.

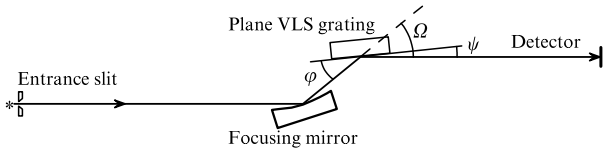

Figure 7. Schematic diagram of a scanning Hettrick–Underwood spectrometer/monochromator. The focusing mirror directs a converging beam onto a plane VLS grating. To minimize the aberrations of the converging beam, the entrance slit is located on the Rowland circle associated with the mirror.

focus of the initial beam in a setup with a constant deflection angle. By requiring that this condition be satisfied for the same p_1 and r'_h for two wavelengths $\lambda_{1,2}$, we obtain a rigid constraint on r'_h:

$$r'_h = r_h \frac{\lambda_2 \sin^2 \psi_1 - \lambda_1 \sin^2 \psi_2}{\lambda_2 \sin^2 \varphi_1 - \lambda_1 \sin^2 \varphi_2} . \tag{17}$$

In this case, coefficient p_1 ceases to be a free parameter,

$$\begin{aligned} p_1 &= \frac{1}{m\lambda_1}\left(-\frac{\sin^2 \varphi_1}{r_h} + \frac{\sin^2 \psi_1}{r'_h}\right) \\ &= \frac{1}{m\lambda_2}\left(-\frac{\sin^2 \varphi_2}{r_h} + \frac{\sin^2 \psi_2}{r'_h}\right), \end{aligned} \tag{18}$$

and in view of the equations $m\lambda_{1,2} = (\cos\varphi_{1,2} - \cos\psi_{1,2})/p_0$, we obtain the relation

$$\frac{r'_h}{r_h} = \frac{(\cos\varphi_2 - \cos\psi_2)\sin^2\psi_1 - (\cos\varphi_1 - \cos\psi_1)\sin^2\psi_2}{(\cos\varphi_2 - \cos\psi_2)\sin^2\varphi_1 - (\cos\varphi_1 - \cos\psi_1)\sin^2\varphi_2} . \tag{19}$$

One can see from expressions (15) and (19) that it is possible to choose the angle of deflection Ω and angles of incidence $\varphi_{1,2}$ (or wavelengths $\lambda_{1,2}$, which is the same thing) at a fixed p_0. After fixing the above parameters, one can arbitrarily choose the dimensions of the instrument (taking into account that r'_h/r_h is already given by relation (19)) and thereby set coefficient p_1 by relation (18). Remarkably, when the grating is rotated, r'_h changes only slightly over a wide wavelength range, including the interval (λ_1, λ_2). In a monochromator with a plane VLS grating, the width of the geometrical image of a point source is less than the diffraction-limited width throughout the operating range, exceeding an octave in wavelength.

The first scanning 6-m-long spectrometer with a plane VLS grating with $p_0 = 1800$ mm^{-1} was developed by the authors of Ref. [12], where ultra-high resolution was demonstrated in a wide wavelength range: $\sim$ 16,000 in the region of $\sim$ 130 Å, $\sim$ 35,000 in the region of $\sim$ 160 Å, and $\sim$ 16,000 in the region of 208 Å. The plate scale was 0.158, 0.125, and 0.071 Å mm^{-1}, respectively. Employed in the measurements were narrow spectral lines of Al IV (130 and 160 Å) and Ne IV (208 Å) ions excited in a glow discharge in a longitudinal magnetic field (Penning discharge). Subsequently, the scanning spectrometer has been repeatedly employed in experiments. Among the most impressive application of instruments of this type is the linewidth measurement of an X-ray laser operating by the transition of Ne-like Se XXV ions (206.38 Å) [31]. It was possible to demonstrate the narrowing of the laser line $\lambda = 206.38$ Å from 50 ± 10 mÅ to 10 mÅ

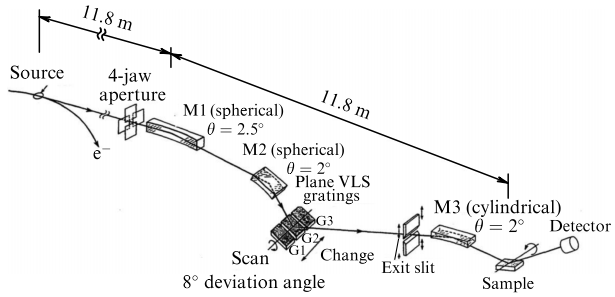

Figure 8. Reflectometer based on a monochromator with replaceable plane VLS gratings (G1–G3), which employs synchrotron radiation: M1, M2 are spherical grazing-incidence mirrors, M3 is cylindrical grazing-incidence mirror, $\Omega = 8°$. (Adapted from Ref. [32].)

upon lengthening the amplifying medium (the length of the plasma of multiply charged Se XXV ions) from 0.5 to 6 cm.

Due to the constancy of the focal length in combination with the constancy of the deflection angle, monochromators of this class have taken a firm place in reflectometers in the SXR channels of synchrotron radiation. One such configuration is depicted in Fig. 8, where the monochromator is part of a reflectometer [32]. To maximize the wavelength range covered (9.5 – 250 Å, or 50–1300 eV), use was made of three replaceable VLS gratings with average line frequencies $p_0 = 300$, 600, and 1200 mm^{-1}.

To study the electronic structure of condensed matter by angle-resolved photoelectron spectroscopy (ARPES), a radiation channel was designed at a synchrotron in Shanghai, including a VLS monochromator for an energy range of 7–791 eV [33]. The VLS monochromator uses three plane VLS gratings with $p_0 = 190$ mm^{-1} (DG1, 7–104 eV), 620 mm^{-1} (DG2, 17–244 eV), and 2000 mm^{-1} (DG3, 55–791 eV). The design of this monochromator is different from that employed in Ref. [32]: the mirror in front of the grating is plane, focusing in the dispersion plane is imposed entirely on the VLS grating, and wavelength scanning is effected by concerted rotation of the mirror and the grating. Though the rated resolving power is wavelength-dependent for each grating, it turns out to be high enough. For gratings DG1–DG3 in the indicated energy ranges, it varies within the limits $(8.3-7.3) \times 10^3$, $(2.4-1.8) \times 10^4$, and $(3.8-2.1) \times 10^4$, respectively.

As is well known, the optimal depth of the groove profile depends on the radiation wavelength. Therefore, to increase the efficiency, in Ref. [33] it is planned to use gratings in which the profile depth varies along the groove (Fig. 9). It is proposed to shift the grating along the z-axis when scanning the wavelength, exposing to the incident beam the grating regions with different profile depths. In practice, a grating with a continuously varying depth will be used.

The synchrotron radiation channel project (National Synchrotron Radiation Laboratory, Suzhou, China) is the same type of thing; it is mainly intended for the study of nanomaterials and their use for energy conversion and storage, as well as for the study of catalysis, using X-ray absorption spectroscopy and optical luminescence under X-ray irradiation [34]. The design energy range (100–1000 eV) contains the K edges of light elements (C, N, O, F) and the L edges of transition metals (Fe, Co, Ni). It is planned to employ two plane VLS gratings with $p_0 = 840$ and 1400 mm^{-1} in the ranges of 60–600 and 100–1000 eV, respectively. The rated resolving power of the monochromator varies in the

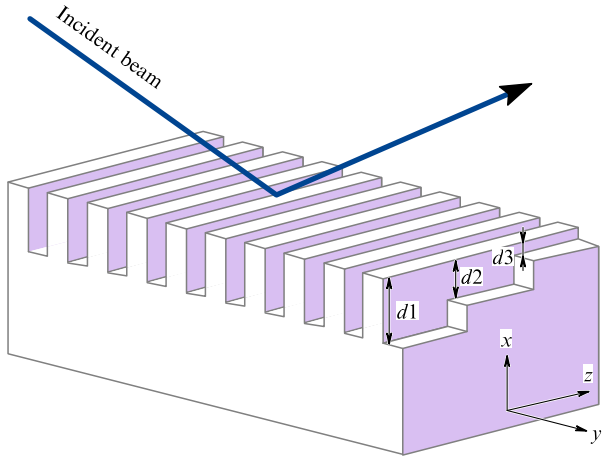

Figure 9. VLS grating with varied groove-profile depth. (Adapted from Ref. [33].)

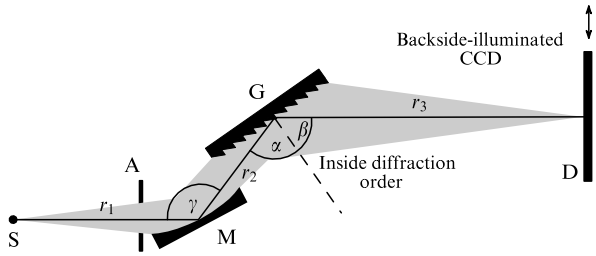

Figure 10. Schematic of a spectrometer based on a flat VLS grating for the range 19–95 Å: S is the radiation source (focus of a synchrotron radiation beam on a thin sample under study), A is an aperture stop, M is a spherical mirror mounted at a grazing-incidence angle of 4° ($\gamma = 172°$), G is a plane VLS grating ($p_0 = 600$ mm^{-1}) with a blaze angle[5] of 1.8° mounted at a grazing angle of 2.1° ($\alpha = 87.9°$) and operating for a grazing-diffraction angle of 5.9° ($\alpha + \beta = \gamma = 172°$). The sensitive detector surface D is perpendicular to the axis of the incident beam. (Adapted from Ref. [36].)

above ranges from ~ 3000 to ~ 1300 for both gratings. As in Ref. [33], the plane VLS grating is the only focusing element of the monochromator, but scanning is performed by rotating only one plane mirror mounted in front of the grating.

Along with the synchrotron source, a laser-plasma source of SXR radiation is also used. In Ref. [35], for instance, a laboratory reflectometer with a constant deflection angle $\Omega = 20°$ was developed, which was designed to characterize the components of projection X-ray microlithography systems. The only focusing element was a VLS grating with $p_0 = 2400$ mm^{-1} with a gold reflective coating made by interference lithography.

5. Spectrometers for recording resonant inelastic X-ray scattering

Resonant inelastic X-ray scattering (RIXS), or resonant X-ray Raman scattering, is used to investigate the electronic structure of molecules, materials, and biological objects. The difference between the energies and momenta of the incident and scattered photons goes to the excitation of the internal degrees of freedom of the material under study. RIXS is a resonant process and is excited, as is X-ray emission spectroscopy, when the photon energy begins to exceed any X-ray absorption edge. The experiment investigates the dependence of the emission spectrum on the energy of exciting photons. The scattered radiation intensity is low, and the experiment requires the use of a high-intensity source of exciting radiation ('photon-hungry' experiment), in particular, third-generation synchrotron radiation sources, and also requires the development of problem-oriented spectrometers that take into account the specifics of the experiment and the radiation source. In the projects known to us, the developers opted for one version or another of the Hettrick–Underwood spectrometer with a plane VLS grating in combination with grazing-incidence focusing optics.

In Ref. [36], a broadband slitless flat-field VLS spectrometer for the spectral region of 130–650 eV (19–95 Å) was developed and demonstrated in operation. The spectrometer is designed, in particular, for the study of radiation-sensitive biological samples placed in a focused synchrotron radiation beam. The slitless spectrometer is constructed according to the Hettrick–Underwood setup and includes a spherical mirror and a plane VLS grating operating in the inside diffraction order (Fig. 10), the mirror directing to the grating a diverging beam rather than a converging one. The instrument records radiation simultaneously (i.e., without any mechanical motion) in the entire operating spectral range with a resolution of at least 1200, provided that the size of the source — a focused monochromatized synchrotron radiation beam — does not exceed 30 μm × 3 mm.

Constructing an RIXS map consists of recording the scattering spectra for a series of fixed values of exciting radiation energy. The high efficiency of the instrument permits recording two-dimensional RIXS maps in several minutes. The spectrometer was optimized for the absorption edges of those elements which organic materials are primarily made up of. The device was designed to record radiation in the vicinity of the L edge of sulfur ($L_{2,3}$, 150 eV) in the first diffraction order, in the vicinity of the K edge of carbon (280 eV) in the second diffraction order, and in the vicinity of the K edges of nitrogen (400 eV) and oxygen (525 eV) in the third diffraction order. Due to the use of three orders of diffraction at different wavelengths, these spectral regions are located rather close to each other on the detector. The procedure for optimizing the configuration parameters was aimed at maximizing the efficiency of scattered radiation collection.

Described in [37] is a flexible approach to the construction of a 200–1000 eV Hettrick–Underwood spectrometer using modular mechanical elements. The chamber design permits operation both in inside and outside diffraction orders. The spectrometer can provide a high resolving power (more than 10^4) for a source size of ~ 1 μm with a $p_0 = 3000$ mm^{-1} grating or a high throughput for moderate resolution.

One of the important research topics using the RIXS method is materials for energy storage devices (batteries), used, notably, in electric vehicles and networked energy storage devices. In terms of energy density, lithium-ion batteries are still considered promising, as they were in the 1990s when the industrial production of $LiCoO_2$/graphite batteries began. Researchers are striving to replace Co with other elements, to improve characteristics, and to reduce the price by forming layers like $LiNi_{1/3}Co_{1/3}Mn_{1/3}O_2$ [37]. The

[5] The blaze angle of a grating with a triangular groove profile is the slope of the working face of the groove relative to the macroscopic surface of the grating.

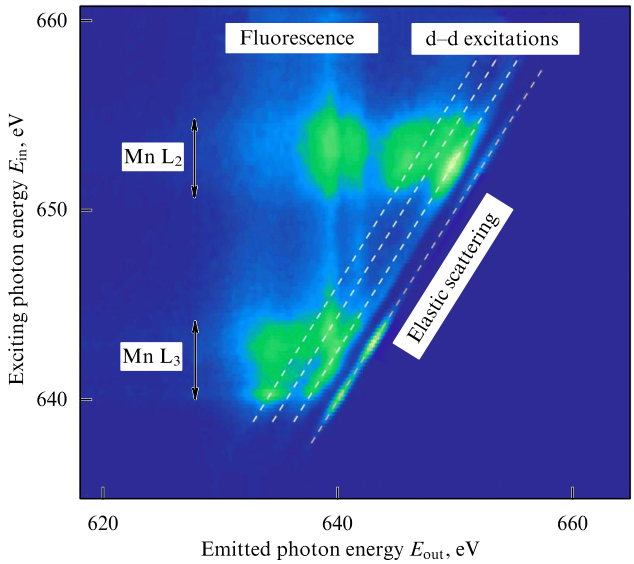

Figure 11. RIXS map obtained in the scanning of exciting photon energy in the vicinity of $L_{2,3}$ Mn absorption edges. The right dashed line shows elastic scattering, and the three other dashed lines correspond to transitions in the 3d shell. Broad vertical bands correspond to nonresonance fluorescence. Material: $LiNi_{1/3}Co_{1/3}Mn_{1/3}O_2$ for Li-ion elements. (Adapted from Ref. [37].)

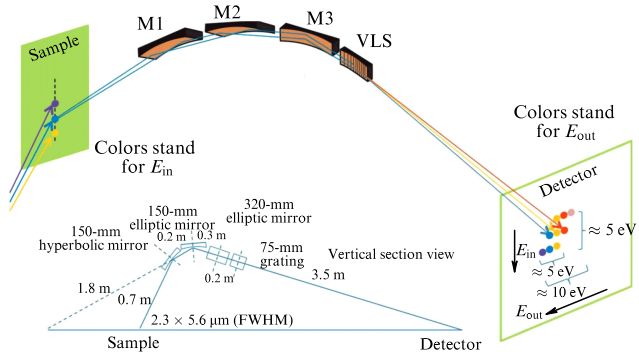

Figure 12. (Color online.) Schematic of an SXR spectrometer with a plane VLS grating for the range 680–740 eV with a spectral resolving power of 30,000: a 150-mm-wide hyperbolic cylinder and a 150-mm-wide elliptical cylinder provide vertical focusing, a 320-mm-wide elliptical cylinder together with a 75-mm-wide VLS grating provide the horizontal one. Bottom: vertical section of the SXR spectrometer layout. (Adapted from Ref. [38].)

potential of X-ray spectroscopy for the study of such materials using the RIXS method has been demonstrated (Fig. 11).

Another experimental approach to recording two-dimensional RIXS maps was described in Ref. [38]. It deals with the development of a complex imaging slitless VLS spectrometer for the 680–740 eV region with a spectral resolution of 30,000. The total length of the VLS spectrometer is about 5 m. A vertically dispersed synchrotron radiation beam with a spectral width of about 5 eV is focused onto an object into a vertical stripe ~ 2 μm wide and ~ 1 mm high. The radiation from the object, which is a source of scattered radiation, is collected and directed onto a plane VLS grating using a system of three grazing-incidence mirrors. The first two mirrors (hyperbolic cylinder and elliptical cylinder) produce the vertical focus of the source on the detector, while the third (elliptical cylinder) focuses the source radiation in the horizontal direction (dispersion plane) and directs the converging beam onto the grating, which decomposes the scattered radiation into a spectrum in the horizontal direction (Fig. 12).

A two-dimensional RIXS map is thereby recorded with the use of X-ray radiation occupying a certain band in the spectrum. The overall magnification of the setup is about 10 in the dispersion plane (horizontal) and about 5 in the crossed direction (vertical). A VLS grating with a blaze angle of 2.8° is mounted at a grazing angle of 8° and operates in the outside order $m = -1$ at a grazing diffraction angle of 2.4°. The use of multilayer-coated gratings is also contemplated.

Note the difference in approaches to recording RIXS maps in Refs [36, 37] and Ref. [38]. The spectrometer designs in Refs [36, 37] imply scanning the wavelength of spectrally narrow exciting radiation near the absorption edge to obtain two-dimensional RIXS intensity maps $I_{sc}(E_{in}, E_{out})$ in coordinates (E_{in}, E_{out}), where E_{in} and E_{out} are the energies of the exciting and scattered radiation, and $I(E_{out})$ is the scattered radiation intensity. In contrast to Refs [36, 37], in Ref. [38] it is assumed that the exciting radiation is spatially dispersed into a spectrum on the sample and that a two-dimensional RIXS map is recorded simultaneously, as shown in Fig. 12.

Another example of the ambitious development of an ultrahigh-resolution RIXS spectrometer based on a plane VLS grating is Ref. [39]. After a thorough analysis of various optical configurations, the authors of the project settled on the Hettrick–Underwood scheme. The recording part of the setup includes a pair of parabolic cylinders for collecting and collimating in the horizontal direction the radiation scattered by the source; a spherical pre-mirror that focuses radiation in the vertical direction behind the VLS grating; an auxiliary plane pre-mirror; and a plane VLS grating, which disperses radiation in the vertical direction. The total length of the setup is 14.5 m. It is assumed that the spectrometer will operate in the 180–2300 eV range and have a resolution of up to 10^5 for $E_{in} \sim 1000$ eV, and the detector will need to be moved when changing the wavelength.

6. VLS gratings for the 'tender' X-ray domain

In a number of studies discussed above, the short-wavelength limit of the working range is in the 'tender' X-ray range. Specifically, a VLS grating with $p_0 = 2500\ \text{mm}^{-1}$ (a version of an ultrahigh-resolution spectrometer in Ref. [39]) is efficient up to $E_{in} = 2300$ eV, which is achieved by mounting the grating at small grazing-incidence angles and applying a gold reflective coating. In Ref. [26], a grating designed for operation in the range of 2–4 keV (6.2 – 3.1 Å) was mounted at a grazing angle of 1.35° and was equipped with an Mo/C multilayer coating.

In Ref. [40], a compact half-meter flat field VLS spectrograph (of Harada class) was designed for X-ray emission spectroscopy in the region of 1–3.5 keV. A spherical ($R = 11.2$ m) VLS grating with $p_0 = 2400\ \text{mm}^{-1}$ and a profile depth of 2.8 nm was mounted at a grazing angle of 1.47° and coated with a Ni/C multilayer mirror consisting of 81 layers. The thicknesses of the two upper layers (Ni and C) were greater than those of the underlying periodic structure with a period of 56 Å, and therefore the multilayer coating could be considered aperiodic [41–43]. The $L\alpha_{1,2}$ X-ray emission lines of the elements Cu, In, Ga, and Se were recorded in the range from 0.9 to 3.3 keV. The resolving power was no

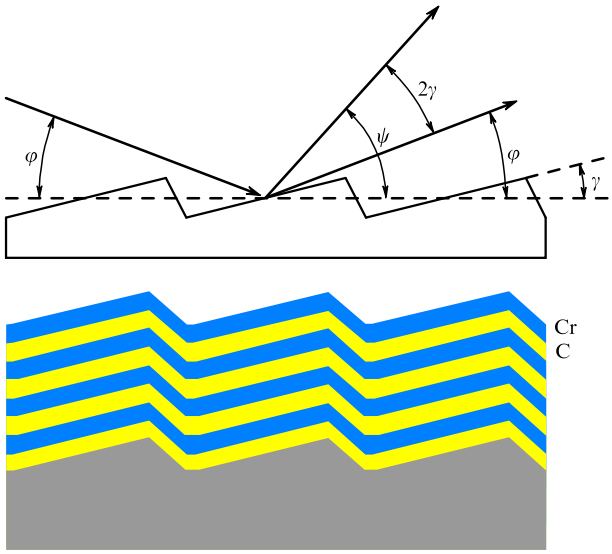

Figure 13. Diffraction by a 'blazed' grating with a Cr/C multilayer coating [46, 47].

higher than 300 and, supposedly, was due to the short grating–detector distance, the small length (~ 8 mm) of the focal field, and the size of the detector pixel.

It should be noted that the use of gratings with a multilayer coating for the vacuum region of the spectrum began at the end of the 20th century (see, e.g., Refs [44, 45]). It is evident that the prospect of moving into the short-wavelength region is associated with the use of gratings with a multilayer reflective coating, which permits operating at much larger grazing-incidence angles without a loss in efficiency and, consequently, increasing the acceptance angle. Of greatest interest, in our opinion, are VLS gratings (as well as gratings with equidistant grooves) with a multilayer coating and a 'blaze angle,' which make it possible, in particular, to get rid of scattered light near the zero order and reflections in undesirable orders. For operation in a broad range of wavelengths and angles of incidence, the grating spacing, the 'blaze' angle, and the period of the multilayer structure must be matched (Fig. 13).

We consider a grating with a multilayer coating and a triangular groove profile (echelette) with a slope angle (blaze angle) γ. Let us consider a preferred grating mount whereby the mth order diffraction angle coincides with the 'blaze' direction. Then, the grating equation (10) gives

$$2\sin\frac{\Omega}{2}\sin\gamma = mp_0\lambda\,, \tag{20}$$

where Ω is the deflection angle and $\Omega = 2(\varphi+\gamma)$, where φ is the grazing-incidence angle. In this case, it is desirable that the reflection from the multilayer structure occur at the maximum of its resonance reflection profile. Disregarding the difference of the refractive index in the layers of the multilayer structure from unity, according to the Bragg–Wolf equation, we have

$$2d\sin\frac{\Omega}{2} = n\lambda\,, \tag{21}$$

where d is the period of the multilayer structure and n is the interference order. Equations (20) and (21) jointly give the

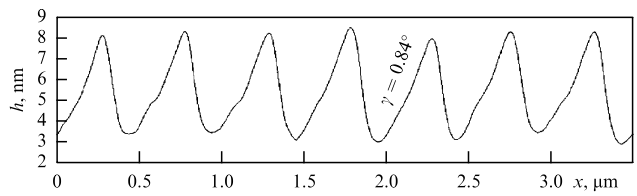

Figure 14. Groove profile of the grating with a blaze angle $\gamma = 0.84°$ and a Cr/C multilayer coating (20 layer pairs with a period of 73 Å) measured with an atomic-force microscope. (Adapted from Ref. [47].)

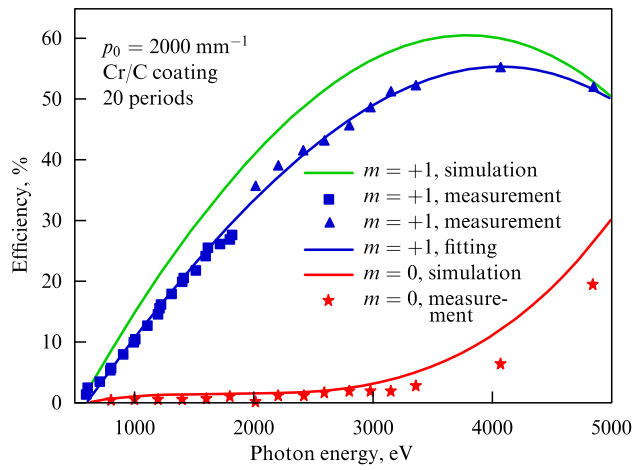

Figure 15. Efficiency of a grating with a blaze angle 0.84°, $p_0 = 2000\ \mathrm{mm}^{-1}$, and a Cr/C multilayer coating. (Adapted from Ref. [46].)

constraint

$$\frac{\sin\gamma}{mp_0} = \frac{d}{n}\,, \tag{22}$$

whereby the multilayer coating may be efficient in a sufficiently broad wavelength interval. In this case, of course, the radiation should be recorded near the diffraction direction $\psi = \varphi + 2\gamma$ (deflection angle: $\Omega = 2(\varphi+\gamma)$), which provides the highest intensity.

Fabricated and investigated in Ref. [46] was a grating ($2000\ \mathrm{mm}^{-1}$) with a multilayer coating (20 periods of Cr/C) intended for operation in the range of 1–5 keV. The measured blaze angle was 0.84° (Fig. 14; Refs [46, 47]), the structure period was 7.3 nm (the relative thickness of the carbon layer in the period $d_{\mathrm{C}}/d = d_{\mathrm{C}}/(d_{\mathrm{C}}+d_{\mathrm{Cr}}) = 0.6$). The grating and multilayer structure parameters satisfy formula (22) with $m = 1$ and $n = 1$. The grating efficiency was measured in the energy range of 1–5 keV ($\lambda \sim 12.4-2.5$ Å) (Fig. 15). The maximum reflectance in the first inside diffraction order was 55%. It was also noted that the first diffraction order is more than 1000 times more intense than orders with $|m| > 1$ and also 20 times more intense than the zero order (the measurement was carried out at an energy of 2.2 keV).

A grating of this type can be used as a dispersing element of a monochromator with a constant (zero) deflection angle, the second element of which is a multilayer mirror with similar structure parameters, operating at a grazing angle $\Omega/2 = \varphi+\gamma$ and efficiently reflecting at the same wavelength as the multilayer diffraction grating (Fig. 16).

A spherical VLS grating with such a coating can be used as a flat-field spectrograph (of Harada class) with a relatively

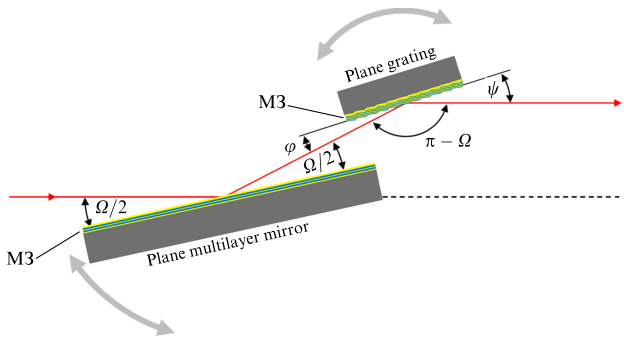

Figure 16. Configuration of a 'tender' X-ray monochromator with a blazed multilayer diffraction grating and a multilayer mirror. The total deflection angle is zero. (Adapted from Ref. [47].)

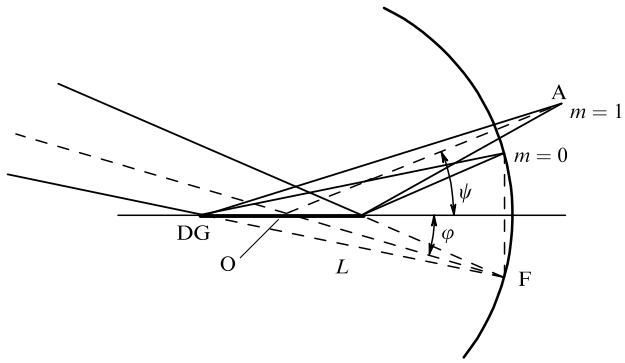

Figure 17. Astigmatism of a plane DG with equidistant grooves in the grazing incidence of a homocentric beam. O is the center of the DG, F is the beam focus, L is the distance OF, and A is the position of the spectral focus in the internal order for a fixed diffraction angle ψ.

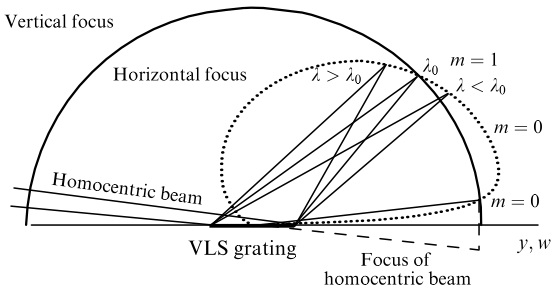

Figure 18. Compensation of astigmatism at one wavelength λ_0 in the incidence of a homocentric beam on a plane VLS grating [16]. The distance between the vertical and horizontal (spectral) foci increases as the wavelength recedes from λ_0.

narrow operating range. Simulations (without including transition layers) show that the spectral profile of the reflectivity of a Cr/C multilayer mirror with 20 periods and a peak reflection coefficient of about 66.4% at a wavelength of about 5.1 Å has a relative width $\Delta\lambda/\lambda \approx 0.086$ (we are talking about the spectral reflectivity profile at a fixed angle of radiation incidence). The working spectral range can be extended by sacrificing the peak reflectance and reducing the number of layers in the multilayer structure. For ten periods and the same layer thickness ratio $d_C/d = d_C/(d_C + d_{Cr}) = 0.6$, the peak reflection coefficient will decrease to 44.6%, and the FWHM will increase to $\Delta\lambda/\lambda \approx 0.14$. Finally, the width can be increased even more by using an aperiodic multilayer structure [41–43].

7. Application of VLS spectrometers in vacuum ultraviolet astronomy

Let a converging homocentric beam be incident on a plane reflective DG with equidistant grooves. As is well known, in the grazing incidence of radiation, such a grating introduces strong astigmatism (Fig. 17), i.e., the spatial positions of the spectral (horizontal) and vertical foci do not coincide. The vertical focus lies on a circle described about point O with a radius L equal to the length of the segment OF — the distance from the grating center to the beam focus.

In internal diffraction orders ($m > 0, \psi > \varphi$), the spectral focus A is outside of this circle (OA > OF) and in external orders ($m < 0$, $\psi < \varphi$), inside of it. The distance from the grating center to the spectral focus of mth order is defined by the formula

$$L_m = L\,\frac{\sin^2\psi_m}{\sin^2\varphi}\,, \tag{23}$$

and the smaller the angle of grazing incidence on the grating, the stronger the astigmatism. Relation (23) follows from Eqn (16) for $p_1 = 0$. It is well known that the use of a VLS grating in a converging beam can eliminate astigmatism at a single wavelength λ_0. Hettrick and Bowyer [48] presented the law of spacing variation of a plane VLS grating, to which a converging homocentric beam is directed, required to bring the spectral focus into coincidence with the vertical one at the selected wavelength λ_0:

$$\frac{1}{p(w)} = d(w) = \frac{m\lambda_0}{\cos\varphi(w) - \cos\psi(w)}\,, \tag{24}$$

where $\varphi(w)$ and $\psi(w)$ are the local grazing angles of incidence and diffraction. The rays emanating from any point with the coordinate w on the y-axis on the grating aperture and lying in the principal plane are diffracted in the desired direction, producing a point image of a point source at wavelength λ_0. In this case, the distance between the spectral (horizontal) and vertical foci increases as the wavelength recedes from λ_0 (Fig. 18).

The use of plane VLS gratings in X-ray astronomy commenced in the 1990s. A spectrometer with three plane VLS gratings was used to obtain a map of extrasolar radiation sources in the far VUV spectral region ($\lambda \sim 70-760$ Å) from the artificial Earth satellite EUVE (Extreme Ultraviolet Explorer, NASA observatory) [49–52].

A converging homocentric beam, which produced the image of a distant source, was formed by a grazing-incidence Wolter–Schwarzschild Type-II telescope with a focal length of 136 cm [49]. Half of its annular aperture fell on a deep-survey detector, and the other half was intercepted by three VLS gratings (1/6 of the aperture each), designed for three spectral subbands, each about an octave wide. The spectral images of extrasolar sources were thereby constructed in three channels (A, B, C). In the spectral channels A (70 – 190 Å), B (140 – 380 Å), and C (280 – 760 Å), use was made of VLS gratings with the size of the ruled area of 80 × 200 mm and the spatial groove frequencies of 1675–3550, 830–1750, and 415–875 mm^{-1}, respectively. The detectors were placed in the focal plane of the telescope. To suppress the unwanted background caused by the scattering of the Ly$_\alpha$ line of hydrogen (1216 Å)

and the UV stellar radiation, a thin-film filter was placed in front of each detector. In addition, placed in front of the telescope were collimators, which limited the field of view and prevented the spectrum from being contaminated by the diffuse radiation of the He I (584 Å) and He II (304 Å) resonance lines.

The EUVE space observatory was successfully launched on June 7, 1992 into an orbit with an altitude of 550 km and an inclination of 28° relative to the equatorial plane of Earth and became the first observatory to observe extrasolar objects in the far VUV and SXR spectral regions. As a result of the nine-year work of the observatory, a large number of radiation sources (734 objects in total) were recorded, their spectra obtained in the far VUV and SXR spectral regions, and catalogs of sources and their spectral lines were published. The literature on this issue is quite extensive (see, e.g., Refs [50–52] and references therein). The general picture, colorfully reproducing the distribution of extrasolar radiation sources in the far VUV and SXR spectral regions, was given in Ref. [53].

In Ref. [54], an imaging spectrograph was designed for solar spectroscopy in the range of 4–26 nm. The instrument consisted of a flat-field spectrograph (of Harada class) with a spherical VLS grating and a three-component telescope, which focused separately in two crossed directions. A parabolic cylindrical (1D) grazing-incidence mirror focused a distant source (the Sun) onto the entrance slit of the spectrograph, and a crossed (1D) two-component grazing-incidence Wolter–Schwarzschild Type-II telescope focused a distant source onto the detector plane. The field of view (in this direction) covered the entire solar disk. This approach was implemented in Ref. [55]. Initially, Ref. [54] dealt with an iridium-coated VLS grating with $p_0 = 2400$ mm^{-1} and $R = 17{,}800$ mm, but Ref. [55] dealt with a 'classical' half-meter Harada spectrograph with a gold-coated grating with $p_0 = 1200$ mm^{-1} and $R = 5649$ mm. One detector pixel (20×20 μm) accounted for a domain with an angular size of 3.5″ in the direction perpendicular to the dispersion plane. A domain with an angular dimension of 34″ was imaged on a 100-μm-wide slit.

8. X-ray spectrometer based on a reflection zone plate

A special place among SXR spectrometers is occupied by an efficient specialized spectrometer based on the radiation reflection from an off-axis (peripheral) portion of a reflective zone plate (RZP) [56]. This optical element resides on a plane substrate and combines reflection, focusing, and dispersion in a three-in-one solution. It can also be classified as a plane two-dimensional VLS grating with curvilinear grooves, which provides focusing in the direction crossed relative to the direction of dispersion. Optical elements of this type will be denoted below as RZP/VLS gratings.

The spectrometer [56] was designed to record weak Mn fluorescence excited, in particular, by an X-ray free electron laser (FEL) pulse in a liquid jet with a low content of Mn atoms. The RZP/VLS grating was optimized for recording the $L\alpha_1$ (637 eV) and $L\beta_1$ (649 eV) fluorescence lines of Mn atoms, and the rated RZP/VLS grating energy of 640 eV (19.4 Å) was chosen in order to capture both lines and enhance the fluorescence signal. When designing the RZP/VLS grating, the goal was to maximize the efficiency and the acceptance angle, which was $3 \times (27 \times 40$ mrad), while the spectral resolution was limited to ~ 100. The grating spacing at the center was ~ 3.5 μm; the angles of incidence and diffraction were (at the center) 2.15° and 1.0° (external diffraction order was used). The grating length was 80 mm, the line frequency varied from 1105 to 79 mm^{-1}, and the angle of incidence varied from 3.9° to 1.5°. The source–grating center and the grating center–focus distances were 90 and 400 mm. The spectrometer involved placing a ~ 120-μm-wide slit in front of the detector.

The RZP/VLS grating was made in the form of three identical strips 2.4 mm wide and 80 mm long, fanning out from the source, on a flat gold-coated silicon wafer. Use was made of the electron beam lithography technique followed by reactive ion etching. The depth of the rectangular profile was 13 nm [56].

The spectrometer was used in an experiment at the Linac Coherent Light Source facility (Fig. 19). Fluorescence emission was excited by a femtosecond pulse (100 fs) from an X-ray laser in a liquid jet containing Mn atoms at a very low density [57]. The use of ultrahigh brightness femtosecond FEL pulses allows data to be obtained before the onset of radiation damage. This is especially important for biological materials and samples in an aqueous solution, for example, for tracking chemical dynamics during catalytic reactions and electron transfer. This approach is called probe-before-destroy. The described spectrometer is intended for X-ray absorption spectroscopy (XAS) at the L edge of Mn with the aim of using it to collect data from Mn-containing metalloenzymes, such as PS II, Mn-catalase, and MnFe-ribonucleotide reductase, by injecting solution samples into the X-ray interaction point.

Figure 19 shows a schematic diagram of an experiment on recording a fluorescence signal from a solid MnO sample in a liquid jet excited by an FEL pulse with energies below (600 eV) and above (653 eV) the Mn L-edge. The signal due to the L-edge of Mn can be separated from the radiation associated with the K-edge of oxygen. It is believed that the determination of the partial fluorescence yield makes it possible to perform time-resolved X-ray spectroscopy of biological samples using an FEL [57].

Studies using RZP/VLS gratings continued to be developed. In particular, Ref. [58] describes a 17-channel SEM-SXES device based on 17 RZP/VLS gratings arranged in a fan on a common plate and covering the range from 50 to 1120 eV. Emission spectra of the elements Li, Be, B, C, N, Ti, V, O, Cr, Mn, Fe, Co, Ni, Cu, Zn, and Ga were obtained, which were excited by the beam of a Zeiss EVO 40 scanning electron microscope. A resolving power $E/\Delta E$ ranging from ~ 80 to 160 was demonstrated.

RZP/VLS gratings were used for NEXAFS (Near-Edge Absorption Fine Structure) spectroscopy near the K absorption edges of carbon and nitrogen [59]. A 1.2-ns SXR pulse from a laser-produced plasma was used. A test sample and a filter were placed in the path between the source and the optical element: in the case of nitrogen, a 200-nm-thick Si_3N_4 membrane and a free-standing 200-nm-thick Al filter; in the case of carbon, a free-standing 112.5-nm-thick polyimide film and a free-standing 200-nm-thick Ti filter. A resolving power $E/\Delta E \sim 950$ was demonstrated near the corresponding absorption edges. The authors believe that the high efficiency of the optical elements makes it possible to study radiation-sensitive biological samples.

In Ref. [60], the SXR spectrum of liquid water was obtained using a spectrometer with an RZP/VLS grating

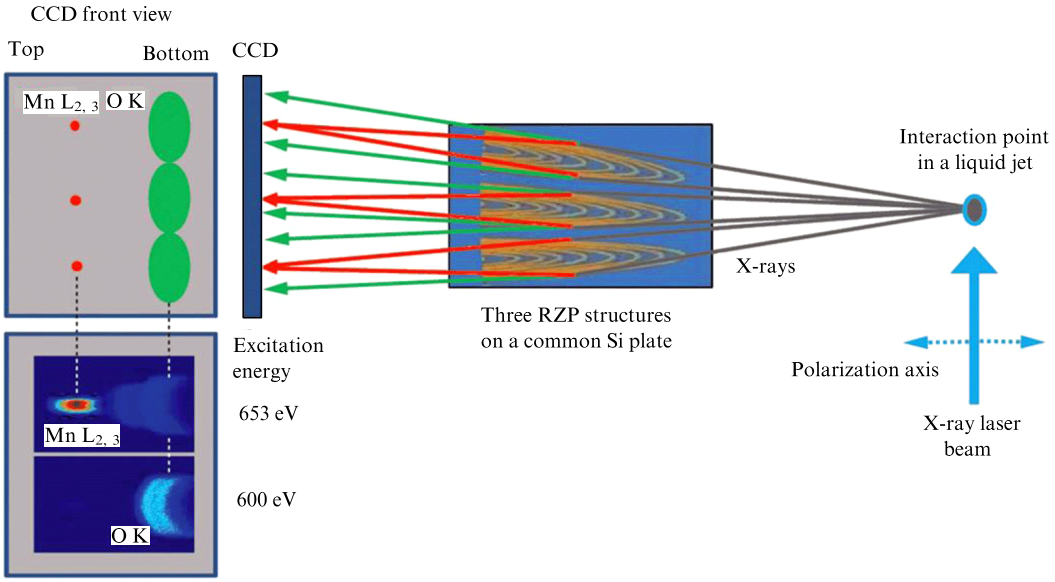

Figure 19. Schematic representation of the experiment with a high-transmission X-ray spectrometer (top view) and the front side of the CCD camera. Left: front view of the CCD with schematic depiction of Mn L-fluorescence focused at the top of the CCD (left in the figure) and O K-fluorescence defocused at the bottom of the CCD (right in the figure). Bottom left: measured images of the fluorescence emission of a solid MnO sample diffracted from one zone plate at an incident photon energy below (600 eV) and above (653 eV) the Mn L-edge. (Adapted from Ref. [57].)

optimized for an energy of 526 eV. The meridional frequency of the lines varied from 2953 to 3757 mm^{-1}. The fluorescence of water (liquid jet in vacuum) was excited by a focused and monochromatized (0.2 or 0.7 eV) synchrotron radiation beam. The spectrometer resolution was estimated at ~ 0.46 eV, which corresponded to $E/\Delta E \sim 1200$. Unlike, for example, the results from Refs [56, 57], a spectral line was formed on the focal surface: in the direction crossed with the direction of dispersion, only minor focusing of the diffracted beam was performed, since the RZP/VLS grating lines had a relatively low curvature.

In concluding this section, we note that the RZP/VLS grating provides a larger acceptance solid angle than more conventional SXR spectrometers do, but the required spectral resolution is realized in a much narrower spectral region. All the dispersion elements discussed in this section were fabricated by electron beam lithography.

9. Domestic soft X-ray VLS spectrometers

Work to develop the first domestic VLS spectrometers and VLS gratings for the vacuum region of the spectrum was commenced at the LPI in 2014 with the support of the Russian Science Foundation. Three high-resolution VLS spectrometers were made and tested: an original imaging (stigmatic) spectrograph for the wavelength range of 12–30 nm; a scanning spectrometer/monochromator of the Hettrick–Underwood type for the range $\lambda \sim 5-30$ nm; and a flat-field Harada spectrograph for the range $\lambda \sim 5-27.5$ nm.

The radiation was recorded by detectors based on back-illuminated CCD arrays with square pixels 13 and 13.5 μm in length. When using VLS gratings manufactured by interference lithography, the spectral resolution was determined by the plate scale and the size of the detector pixel. In all cases, the diffracted radiation was incident on the focal curves almost along the normal, which made them perfectly compatible with modern CCD detectors.

Sections 9.1–9.3 briefly describe the designs and characteristics of the three spectrometers, and Section 10 describes a method for the fabrication of domestic VLS gratings.

9.1 Imaging (stigmatic) spectrograph for a wavelength range of 12–30 nm

The problem of obtaining spectra with spatial resolution and, more generally, constructing spectral images arises in the study of laboratory/solar plasmas and laboratory sources of SXR radiation. Examples of recently developed objects requiring the use of imaging (stigmatic) spectrometers are a source of high (even and odd) harmonics in a relativistic helium plasma produced by a multiterawatt femtosecond laser [18–20], as well as a relativistic 'flying mirror': a source of SXR radiation arising from the reflection of the radiation of a femtosecond laser from a relativistic plasma excited by pulses of a multiterawatt laser [61]. Such objects require a spatial resolution of ~ 1 μm.

Our goal was to design a high-resolution imaging laboratory spectrometer that retains stigmatism over a wide (on the order of an octave) wavelength range [62–65]. Compared with grazing-incidence reflective optics, normal incidence optics have low aberrations for a relatively large field of view and input acceptance angle. Their use in the SXR range became possible due to the advent of X-ray multilayer mirrors (MMs) and, in particular, broadband MMs based on aperiodic multilayer structures [15, 41, 42], which provide a sufficiently high reflection coefficient at normal incidence.

As indicated in Section 7, when a homocentric beam is incident on a plane VLS grating, the stigmatism condition can be met at a single wavelength λ_0 (see Fig. 18). When a weakly astigmatic beam is incident on a plane VLS grating, the condition of strict stigmatism can be fulfilled simultaneously at two wavelengths, λ_1 and λ_2 (this condition is fulfilled strictly for paraxial rays in the principal plane). With the proper choice of λ_1 and λ_2, the condition of practical stigmatism is fulfilled in an interval of about two octaves in wavelength. The term 'practical stigmatism' means that the

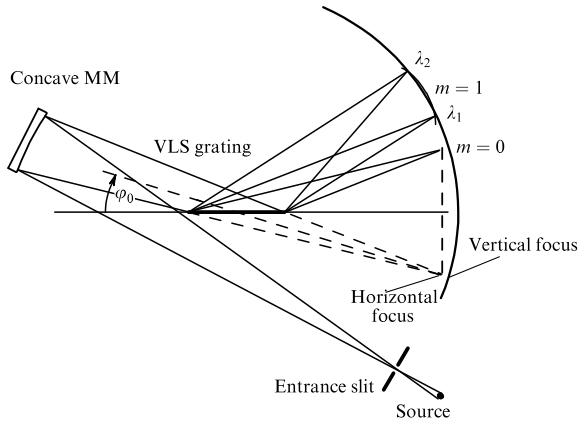

Figure 20. Schematic of a broadband imaging spectrometer comprising a concave focusing aperiodic MM and a plane VLS grating.

image of a point monochromatic source obtained by the numerical ray tracing method almost entirely fits into the size of the detector pixel (a square with a side of 13 μm in our case).

Let us assume that the frequency of VLS-grating lines is described by Eqn (1). Let a weakly astigmatic beam be incident on the grating, L_h and L_v denote the distance from the grating center to the horizontal and vertical foci, φ and ψ stand for the grazing angles of incidence and diffraction of the central ray, and r'_h and r'_v denote the distances from the grating center to the horizontal and vertical (paraxial) foci upon diffraction. We require that $r'_\mathrm{h} = r'_\mathrm{v}$. Then,

$$\frac{L_\mathrm{h} \sin^2 \psi}{\sin^2 \varphi + m p_1 \lambda L_\mathrm{h}} = L_\mathrm{v} \,. \tag{25}$$

Jointly with the grating equation $\cos\varphi - \cos\psi = m\lambda p_0$ (10) for the central ray, Eqn (25) defines the stigmatism condition at a wavelength λ. At this stage, φ and p_0 are free parameters. Next, we impose the condition of stigmatism simultaneously at two wavelengths, λ_1 and λ_2, and express p_1 from Eqn (25) as

$$p_1 = \frac{1}{m\lambda_1}\left[-\frac{\sin^2\varphi}{L_\mathrm{h}} + \frac{\sin^2\psi_1}{L_\mathrm{v}}\right] = \frac{1}{m\lambda_2}\left[-\frac{\sin^2\varphi}{L_\mathrm{h}} + \frac{\sin^2\psi_2}{L_\mathrm{v}}\right] . \tag{26}$$

On rearrangement, we arrive at a constraint between φ and p_0:

$$\varphi = \arcsin\left(\frac{m p_0 \sqrt{\lambda_1 \lambda_2}}{\sqrt{L_\mathrm{v}/L_\mathrm{h} - 1}}\right) . \tag{27}$$

This signifies that astigmatism may be eliminated simultaneously at two wavelengths at the sacrifice of one of the free parameters (φ or p_0). For the first implementation of the spectrograph, we adopted the customary figure $p_0 = 600\ \mathrm{mm}^{-1}$ and a one-meter mirror radius.

Here, a remark is in order. The grazing angle φ should be small enough to provide a sufficiently high grating reflectivity. This requirement is fulfilled even when the operating range amounts to about two octaves in wavelength, since $p_0\sqrt{\lambda_1\lambda_2} \sim 2p_0\lambda_1 \sim 1.7 \times 10^{-2} \ll 1$, and the value of $L_\mathrm{v}/L_\mathrm{h} - 1 < 1$ is controllable.

The remaining parameters p_i $(i = 2, 3, \ldots)$ of the plane VLS grating are derived by expanding into a Taylor series the

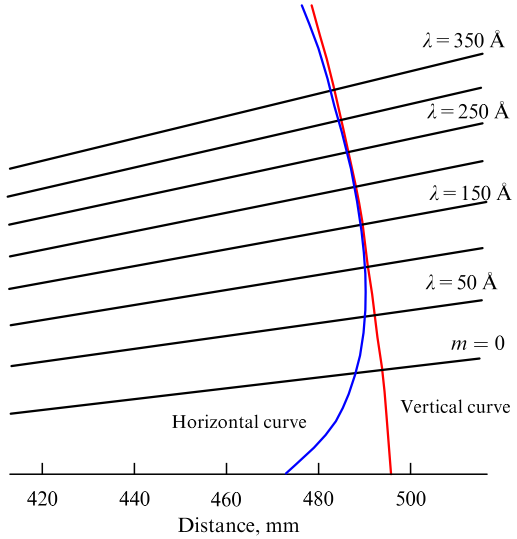

Figure 21. Vertical and horizontal (spectral) focal curves of the spectrograph. Plotted on the abscissa is the distance from the grating center. Straight lines stand for the paths of diffracted central rays of different wavelengths. The curves intersect at the wavelengths $\lambda_1 = 144$ Å and $\lambda_2 = 270$ Å. The range of 'practical stigmatism' amounts to two octaves in wavelength, from approximately 90 to 360 Å [64].

expression

$$m p(w) \lambda_\mathrm{opt} = \cos\left[\operatorname{arccot}\left(\cot\varphi - \frac{w}{L_\mathrm{h}\sin\varphi}\right)\right] - \cos\left[\operatorname{arccot}\left(\cot\psi - \frac{W}{L_\mathrm{v}\sin\psi}\right)\right] . \tag{28}$$

The meridional coma is compensated at a wavelength λ_opt when p_2 satisfies the equation

$$m\lambda_\mathrm{opt}\, p_2 = \frac{3}{2}\left(-\frac{\sin^2\varphi\cos\varphi}{L_\mathrm{h}^2} + \frac{\sin^2\psi\cos\psi}{L_\mathrm{v}^2}\right) , \tag{29}$$

and spherical aberration is compensated at a wavelength λ_opt when p_3 satisfies the equation

$$m\lambda_\mathrm{opt}\, p_3 = \frac{\sin^2\varphi}{L_\mathrm{h}^3}\left(-2\cos^2\varphi + \frac{\sin^2\varphi}{2}\right) + \frac{\sin^2\psi}{L_\mathrm{v}^3}\left(2\cos^2\psi - \frac{\sin^2\psi}{2}\right) . \tag{30}$$

Angles φ and ψ are related to λ_opt by the grating equation. The wavelength λ_opt in Eqns (29) and (30) is not necessarily the same. In the implementation of the spectrograph, we set $\lambda_\mathrm{opt} = \lambda_1$.

The spectrograph configuration is depicted in Fig. 20. The weakly astigmatic converging beam is formed by a normal-incidence broadband spherical MM based on an aperiodic Mo/Si multilayer structure [15, 41, 42, 66] ($R = 1$ m) deposited in V V Kondratenko's laboratory (National Technical University, Kharkiv Polytechnic Institute, Ukraine). In the 125–250 Å range, the measured reflection coefficient varied between 18 and 13% to decrease to $\sim 8\%$ at 304 Å [66]. Proceeding from the spectral range of the MM (approximately 125–300 Å), in the design of the instrument we adopted $\lambda_1 = 144$ Å and $\lambda_2 = 270$ Å, which minimized the geometrical defocusing on the plane detector surface in the spectral range of the MM. The behavior of the focal curves is shown in Fig. 21. The VLS grating was located approxi-

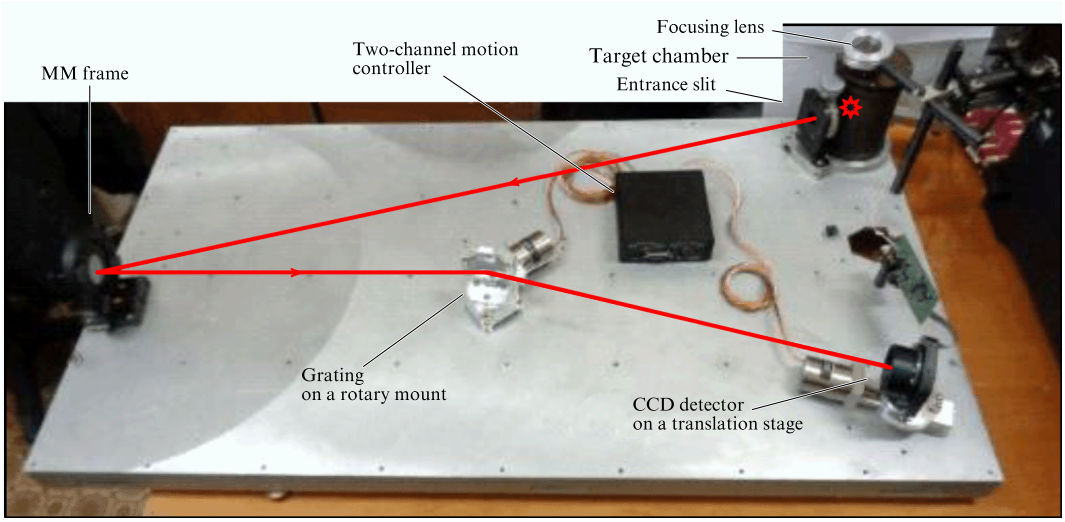

Figure 22. Elements of the spectrograph arranged on a duraluminum plate measuring 1.1 × 0.6 m.

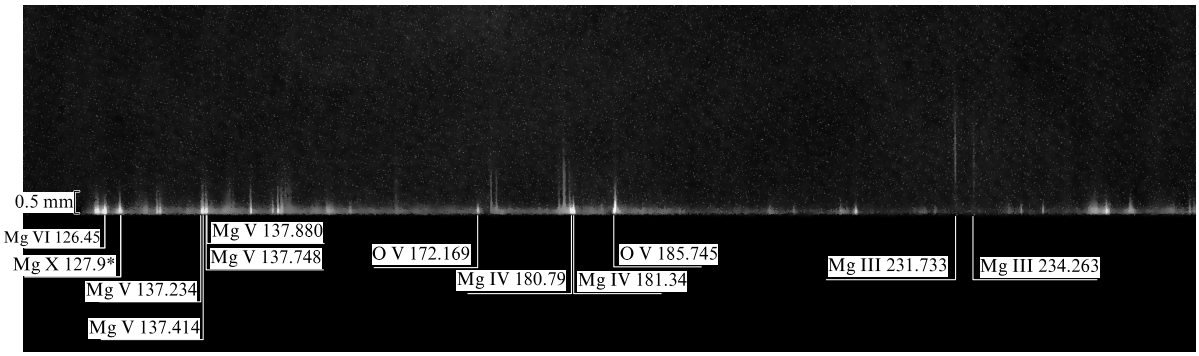

Figure 23. Magnesium plasma spectrum recorded in one laser shot. The spatial resolution vertically (along the target normal) is two detector pixels. The light–shadow boundary corresponds to the surface of the solid target [64].

mately half way between the MM and the detector. A gold-coated VLS grating (55 × 25 mm) with coefficients $p_0 = 600$ mm^{-1}, $p_1 = 2.2$ mm^{-2}, and $p_2 = 6.0 \times 10^{-3}$ mm^{-3} was made using the interference lithography technique in the Scientific and Production Association, State Institute of Applied Optics, Kazan. A photograph of the spectrograph is shown in Fig. 22.

The spectrograph can be used in two modes: (i) the radiation source is imaged onto the entrance slit, which is considered a source, and the spectrograph constructs the stigmatic spectral images of the slit; (ii) the radiation source is placed several centimeters in front of the slit, and the instrument constructs the plasma spectra with vertical spatial resolution. The difference between the two configurations consists of a small difference between the angles of incidence on the MM. Numerical ray tracing showed that the instrument function of the device almost completely fits (both in the vertical direction and in the direction of dispersion) in the detector pixel size (13 μm) in the entire operating range (120 – 300 Å) for a solid acceptance angle of $\sim 4 \times 10^{-4}$ sr and a vertical field of view of ±1 cm [62, 64]. The average plate scale is 6 Å mm^{-1}. We have implemented configuration (ii) and recorded line spectra of laser plasma excited by a focused laser pulse (0.5 J, 8 ns, 1.06 μm). To do this, the spectrograph was placed in a vacuum chamber 3.8 m long and 0.9 m in diameter, evacuated to a pressure of 5×10^{-5} Torr.

By way of example, Fig. 23 shows the spectrum of a magnesium target recorded in one laser shot. The target plane was parallel to the dispersion plane. The detector was a CCD array with 2048 × 1024 square pixels 13 μm in length. The spectral resolving power measured from the spectrum was $\lambda/\delta\lambda \approx 10^3$. The spatial resolution, estimated from the light–shadow boundary, was 26 μm. Both figures correspond to two detector pixels, which is consistent with the data of numerical ray tracing.

Therefore, a new method for obtaining stigmatic spectral images in a wide spectral region in the SXR range has been demonstrated, which consists of using the diffraction of a weakly astigmatic beam by a plane VLS grating, where the incident beam is formed by a normal-incidence broadband aperiodic MM. This approach can certainly be extended to the short-wavelength region down to 111 Å due to beryllium-containing (for example, Mo/Be) normal incidence MMs, which are capable of providing a reflectivity plateau at a level of ~ 0.2 in the range of 111 – 135 Å [67, 68]. This approach can supposedly be extended down to 66 Å due to La-containing mirrors, which provide (in simulations) reflection coefficients of ~ 4% in the range of 66 – 110 Å and ~ 8% in the range of 88 – 110 Å [42].

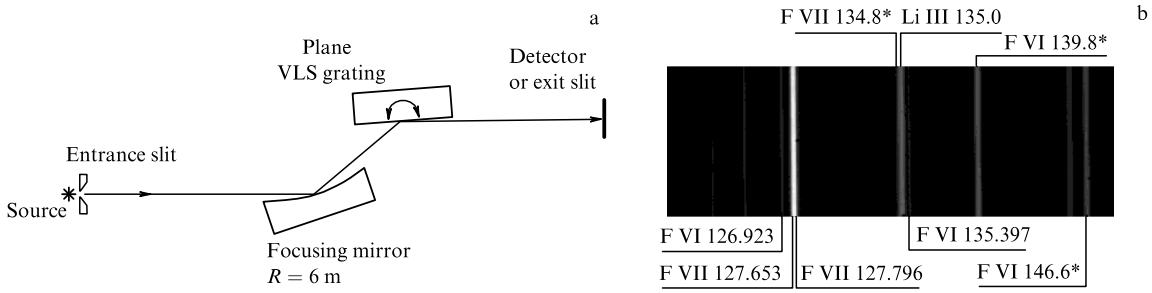

Figure 24. (a) Schematic of a scanning spectrometer/monochromator, (b) portion of the LiF plasma spectrum recorded in the scanning spectrometer mode for a fixed angle of grating rotation. Slit width: 10 μm. Wavelengths are given in Angstroms. Asterisks indicate unresolved line arrays.

9.2 Scanning spectrometer/monochromator for a wavelength range of ~ 5–33 nm

A plane VLS grating with the same parameters as the grating used in the imaging spectrograph (see Section 9.1) was employed in a scanning spectrometer/monochromator of the Hettrick–Underwood class [69] (Fig. 24a). Its configuration comprises an Au-coated spherical mirror ($R = 6$ m) mounted at a grazing angle of 8.34°, which produces the horizontal focus of the image of the entrance slit at a distance of 533.7 mm behind the VLS grating. The grating operates in an external diffraction order with a constant deviation angle of 16.68°, so that the total deviation angle is zero. The instrument can be used either as a flat-field scanning spectrometer with a plate scale of ~ 3 Å mm^{-1} (on average) or as a monochromator with an exit slit. The grating–detector distance (or the distance from the exit slit to the grating) is 532.6 mm. The focal length is precisely equal to this distance at wavelengths of 140 and 273 Å. The focal length hardly depends on the wavelength, so that in the $\lambda < 330$ Å range the geometrical defocusing is less than 13 μm and is below the diffraction limit (Fig. 25). The short-wavelength limit of the operating range is determined by the source brightness rather than defocusing.

The spectrometer was assembled on a two-meter-long optical seat and accommodated in a vacuum chamber (see Section 9.1). The radiation was recorded by a Greateyes detector, Germany (2048 × 512 square pixels 13.5 μm in size).

The instrument was tested in the scanning spectrometer mode by recording the line spectra from laser-produced plasmas of LiF, Mg, and polyethylene targets. Figure 24b depicts a portion of the LiF-plasma spectrum in the region of 120 – 150 Å. In the spectrum of carbon plasma, it was possible to resolve the fine structure (0.14 Å) of the H_α line ($3 \to 2$, 182 Å), which testifies to a resolving power of 1300 at this wavelength.

9.3 Flat-field spectrometer for a wavelength range of 5–27.5 nm

Spectrographs of the Harada class employ one optical element: a grazing-incidence spherical VLS grating (see Fig. 3). In our earlier study [17], three Harada-type spectrographs about 0.25, 0.5, and 1.5 m in length were designed for operation in the ranges of 90–250, 50–275, and 20 – 110 Å, respectively. For experimental implementation, we opted for the half-meter-long VLS spectrograph with an average linear dispersion of 0.18 mm Å^{-1} in the range $\lambda \sim 50 - 275$ Å [70]. The plate scale at a wavelength of 150 Å is 6.28 Å mm^{-1}. The main rated parameters of the spectrograph and the VLS grating are collected in Table 2. The groove frequency of the VLS grating is described by polynomial (1). The groove frequency (1) should vary from 1027.5 to 1427.5 lines mm^{-1} between the edges of the 50-mm aperture. Parameters p_2 and p_3 were selected in such a way as to cancel aberrations at $\lambda_{\rm opt} = 125$ Å. In order to fabricate the VLS grating using the interference lithography technique, an algorithm was developed for designing the writing configuration with an

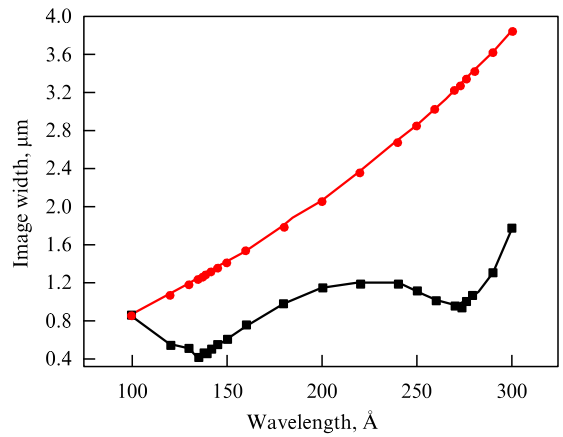

Figure 25. Width of an image of a point monochromatic source caused by the combined action of geometrical defocusing and aberrations and obtained by numerical ray tracing (black squares). One can see that the width of these images does not exceed the diffraction-limited image width (red dots). When moving to longer wavelengths, the diffraction-limited width grows faster than the wavelength: in this case, the diffraction angle ψ and the aperture of diffracting beam $W \sin\psi$ (W is the width of the VLS grating) become smaller.

Table 2. Rated parameters of the spectrograph configuration and the VLS grating [70].

Radius of curvature of spherical grating R, mm	6000
Grating diameter D, mm	60
p_0, mm^{-1}	1200
p_1, mm^{-2}	8.0
p_2, mm^{-3}	0.044
p_3, mm^{-4}	2.28×10^{-4}
Grazing-incidence angle φ, deg	3.0
Aberration compensation wavelength $\lambda_{\rm opt}$, Å	125
Entrance slit–grating center difference r, mm	252
L, mm	250

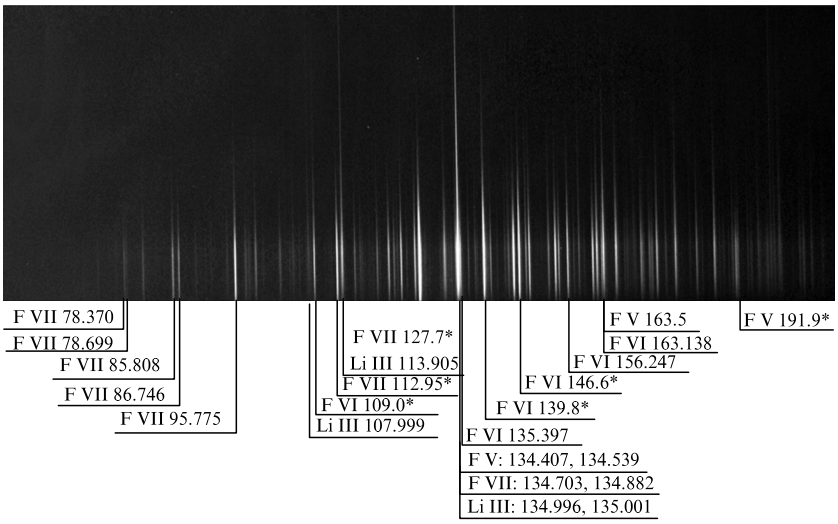

Figure 26. Spectrum of Li III and F V–FV II ions (LiF target). Asterisks denote unresolved line arrays [70].

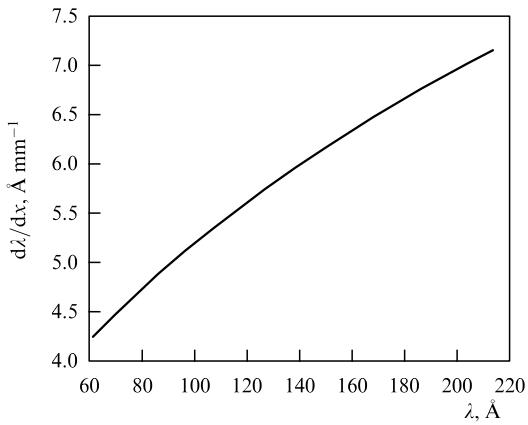

Figure 27. Plate scale of the flat-field VLS spectrograph [70].

auxiliary spherical mirror-aberrator (the solution to the inverse problem of interference lithography) (see Section 10 below).

When testing the spectrograph, line spectra were recorded from the laser plasma of lithium fluoride and Teflon targets excited by a focused laser beam (0.5 J, 8 ns, 1.06 μm). A resolving power $\lambda/\delta\lambda = 800$ was demonstrated in the wavelength region of 135 Å. Figure 26 shows a photograph of the spectrum obtained in one laser shot in the irradiation of the LiF target and containing the lines of Li III and F V–F VII ions. The half-widths (FWHM) of separate lines correspond to two detector pixels. The practical spectral resolution is limited by the spatial resolution of the detector and is numerically equal to the product of the plate scale and the doubled CCD pixel size (26 μm). Since dispersion is wavelength-dependent (Fig. 27), the spectral resolution is also wavelength-dependent. The theoretical resolving power corresponding to two detector pixels depends on the wavelength and varies from 550 in the region of 60 Å to 1170 in the region of 220 Å.

10. VLS-grating fabrication technologies

Programmable mechanical ruling engines, the method of interference lithography, and, more recently, electron beam lithography are used for the production of VLS gratings throughout the world.

In 1975–1976, Harada et al. (Central Research Laboratory, Hitachi, Tokyo) [7, 71] reported the implementation of a programmable ruling engine capable of both varying the groove spacing on the grating aperture according to a given law and producing both straight and curved grooves. The minimum increment of the grating spacing was 0.2 Å [8]. After improving his ruling engine, Harada was able to produce gratings up to 300 mm wide with up to 200-mm-long grooves with an average groove frequency of up to 10^4 mm^{-1} [10].

Hitachi was apparently historically the first manufacturer of commercially available VLS gratings. An advertisement for VLS gratings can be seen on the website of Hitachi High Technologies America, Inc. (USA) [72]. A photograph of a demo sample is presented on the company's website and in advertising brochures, in which the interval between grooves varies from 0.3 to 1.7 μm with an increment of 500 Å. The photograph was taken using a scanning electron microscope. At present (after Harada left Hitachi), the company produces only replicas from the existing ruled master gratings.

There are reports about the manufacture of plane ruled gratings by Carl Zeiss Optronics GmbH (Germany) on the programmable ruling engine GTM6 [36]. The engine is currently at the disposal of the Helmholtz-Berlin Center for Materials and Energy (Helmholtz-Zentrum Berlin für Materialien und Energie).

Electron beam lithography is used for the manufacture of single samples of VLS gratings. The method involves exposing the resist to an electron beam, followed by plasma-chemical etching. The electron beam applies the required 'pattern' of VLS-grating lines to the resist. Then, the exposed resist is developed and etched away, after which the grating material is etched away in the exposed areas, thereby transferring the 'pattern' to the grating material. In the last step, the remaining protective resist is removed. Using this method, the first domestic VLS grating for the SXR spectral region was fabricated at the Center for Collective Use of the Moscow Institute of Physics and Technology (Dolgoprudny), which is a laminar structure with a duty cycle of ~ 0.5 (Fig. 28) [63]. The VLS grating pattern was made in a 100-nm-thick tungsten film deposited on a K8 glass substrate.

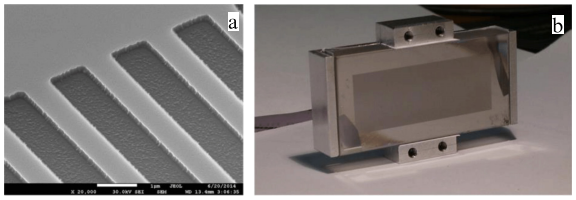

Figure 28. (a) Photograph of a portion of a tungsten VLS grating with $p_0 = 600$ mm^{-1} obtained with a scanning electron microscope and (b) photograph of the grating with a (ruled) area of 40 (w) × 16 (h) mm in a frame.

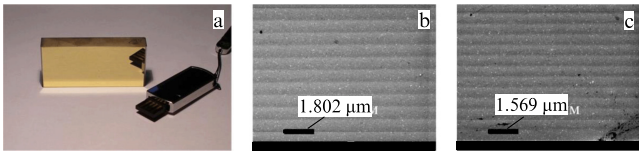

Figure 29. Gold-coated VLS grating 55 (w) × 25 (h) mm in size made by interference lithography at a wavelength of 532 nm. (a) Appearance of the plane VLS grating with a line density of 600 mm^{-1} at the center of the aperture, (b, c) images of the portions of the VLS grating at the opposite ends of the aperture obtained with a scanning electron microscope.

An electron beam writes a grating pattern with nanometer precision on an area several hundred microns in width and length. In the manufacture of large gratings, the problem arises of matching different exposure areas during the stage translation, the solution to which determines the quality of the grating. There are electron beam lithography devices that provide a positioning accuracy up to two nanometers over an area of 80 × 10 mm.

The problem of matching exposure fields does not arise when using the method of interference lithography, when the required 'pattern' is written on the photoresist with the interference of two coherent beams, and the dependence of the frequency of interference fringes on the substrate aperture should be described by polynomial (1) with the previously found coefficients p_0, p_1, p_2, and p_3. Also of importance is the radius of curvature of the interference fringes. The optical lithographic scheme is found in the solution to the inverse problem of interference lithography (i.e., in the determination of an optical configuration that approximates the required distribution (1) by the spatial frequency of the interference fringes), which is a nontrivial problem. In many (but not all) cases, it is sufficient to use a recording scheme consisting of two point coherent sources and one auxiliary oblique-incidence spherical mirror, which introduces controlled aberrations into the wavefront of one of the interfering beams. If the wavelength of the laser radiation is fixed, then seven unknowns appear in the problem (the radius of the auxiliary mirror, three distances, and three angles). When solving the inverse problem, it is useful to use the solution to the direct problem of interference lithography [73].

Interference lithography is currently one of the most technologically available methods of manufacturing VLS gratings. It is believed that gratings made by interference lithography have less radiation scattering than those made on a mechanical ruling engine. Similar problems were successfully solved in Japan in the manufacture of VLS gratings for a spectrograph with a flat focal field [74]. VLS gratings fabricated by interference lithography are commercially available (for example, Shimadzu gratings (Shimadzu, Japan) [75]), and the calculation of the VLS grating writing scheme is facilitated for problems similar to those already solved. A turnkey solution to the task of making a VLS grating is provided by Horiba Jobin Yvon (Horiba branch in France).

To make the first domestic plane VLS grating for the SXR spectral region by interference lithography, use was made of 532-nm radiation (Scientific and Production Association, State Institute of Applied Optics, Kazan) (Fig. 29) [16]. Figure 29b shows sections of a flat VLS grating at opposite ends of the aperture, obtained with a scanning electron microscope. This grating has been used successfully in the

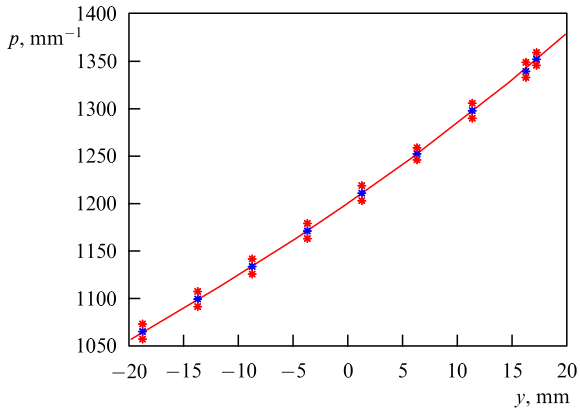

Figure 30. Rated (curve) and measured (asterisks) groove frequency of a spherical VLS grating [70].

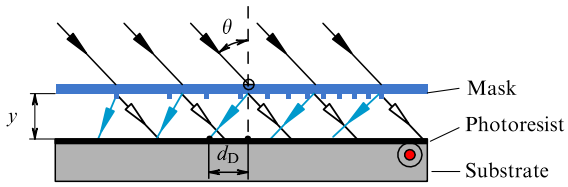

Figure 31. Setup for 'copying' a master VLS grating with $p_0 = 3600$ mm^{-1} by interference lithography at a wavelength of 325 nm. Incidence angle of laser radiation $\theta = 35.5°$, air gap thickness $y = 3$ mm, $d_D = 2.188$ mm is the shift of the grating center with $p_0 = 3600$ mm^{-1}. The −1st-order diffraction is shown in blue. (Adapted from Ref. [76].)

imaging spectrograph (see Section 9.1) and in the scanning spectrometer/monochromator (see Section 9.2). The first domestic spherical VLS grating ($R = 6000$ mm) was also made at the Scientific and Production Association, State Institute of Applied Optics, Kazan, and the calculation of the recording scheme at a wavelength of 532 nm was performed at the Lebedev Physical Institute [70]. The measured variation in the groove frequency in the VLS-grating aperture and the spectrograph parameters based on it ideally coincided with the rated ones (Fig. 30).

It is valid to say that the foundations of the interference-lithographic technology of VLS gratings for the SXR spectral region were laid jointly by the LPI and the State Institute of Applied Optics.

An interesting method of 'copying' plane VLS gratings with a high line frequency using the method of interference lithography was proposed and implemented in Ref. [76]. The initial master grating was a VLS grating with $p_0 = 3600$ mm^{-1}, which was made by the method of

electron beam lithography. It was used as a transmission phase mask for the diffraction of 325-nm-wavelength laser radiation directed onto a photoresist-coated substrate at an angle of 35.5°. The interference pattern arose in the interference of the only possible zero and −1st diffraction orders (Fig. 31). In this case, the distribution $p(w)$ on the photoresist slightly differs from the distribution on the initial master grating. One of the advantages of the method is the possibility of translation of the photoresist-coated substrate along the grating grooves during exposure and, therefore, the possibility of using a master grating with a short groove, whose fabrication does not consume much time of the electron-lithographic facility.

11. Conclusions

This brief review is devoted to SXR spectrometers based on plane and concave grazing-incidence VLS gratings — reflective DGs with a spacing that monotonically changes across the aperture according to a given law. These aperiodic elements of the optics and spectroscopy of the SXR range are the product of modern high technologies. They have a number of advantages over classical gratings with equidistant grooves, and their combination with other optical elements (MMs, grazing-incidence aspherical mirrors, etc.) in one instrument opens up new possibilities for research. In particular, VLS gratings form flat-field spectral images, which makes them perfectly compatible with modern CCD detectors. VLS spectrometers/monochromators, designed according to the Hettrick–Underwood configuration and its derivatives, have a constant focal length and deflection angle. Due to these properties, various VLS spectrometers and VLS monochromators have taken a firm place in modern physics experiments.

Domestic development in this area began relatively recently, thanks to a grant from the Russian Science Foundation (2014). The first domestic flat-field spectrometers were made at the Lebedev Physical Institute, RAS (see Sections 9.1–9.3). Solving new problems often calls for the use of dedicated VLS spectrometers which take into account the special features of the scientific problem and the radiation source. This requires a full cycle of instrument development: design and optimization of the closed optical configuration source–spectrometer–detector, including the calculation of the parameters of the VLS grating and (when necessary) auxiliary mirrors, and fabrication of the VLS grating and the VLS spectrometer as a whole. The Lebedev Physical Institute has accumulated experience in the design of VLS spectrometers and, jointly with the State Institute of Applied Optics, has laid the foundations of VLS-grating technology using the method of interference lithography.

Acknowledgements. This study was supported by the Russian Foundation for Basic Research (grant no. 19-12-50059).

References

1. Rowland H A *Phil. Mag.* **13** 469 (1882)
2. Samson J A R *Techniques of Vacuum Ultraviolet Spectroscopy* (New York: Wiley, 1967)
3. Schumann V *Akad. Wissenschaften Wien* **102** (2A) 625 (1893)
4. Mack J E, Stehn J R, Edlén B *J. Opt. Soc. Am.* **22** 245 (1932)
5. Edlén B *Rep. Prog. Phys.* **26** 181 (1963); Translated into Russian: *Usp. Fiz. Nauk* **89** 483 (1966)
6. Cornu M A *C.R. Acad. Sci.* **117** 1032 (1893)
7. Harada T, Moriyama S, Kita T *Jpn. J. Appl. Phys.* **14** (S1) 175 (1975)
8. Harada T, Kita T *Appl. Opt.* **19** 3987 (1980)
9. Kita T et al. *Appl. Opt.* **22** 512 (1983)
10. Kita T, Harada T *Appl. Opt.* **31** 1399 (1992)
11. Hettrick M C, Underwood J H *AIP Conf. Proc.* **147** 237 (1986)
12. Hettrick M C et al. *Appl. Opt.* **27** 200 (1988)
13. Underwood J H, Attwood D T *Phys. Today* **37** (4) 44 (1984); Translated into Russian: *Usp. Fiz. Nauk* **151** 105 (1987)
14. Namioka T *J. Opt. Soc. Am.* **49** 446 (1959)
15. Ragozin E N, Vishnyakov E A, Kolesnikov A O, Shatokhin A N *Aperiodicheskie Elementy v Optike Myagkogo Rentgenovskogo Diapazona* (Aperiodic Elements in Soft X-ray Optics) (Ed. E N Ragozin) (Moscow: Fizmatlit, 2018)
16. Ragozin E N et al. *Proc. SPIE* **10235** 102350L (2017)
17. Vishnyakov E A, Kolesnikov A O, Ragozin E N, Shatokhin A N *Quantum Electron.* **46** 953 (2016); *Kvantovaya Elektron.* **46** 953 (2016)
18. Pirozhkov A S et al. *Phys. Rev. Lett.* **108** 135004 (2012)
19. Pirozhkov A S et al. *New J. Phys.* **16** 093003 (2014)
20. Pirozhkov A S et al. *Sci. Rep.* **7** 17968 (2017)
21. Neely D et al. *AIP Conf. Proc.* **426** 479 (1998)
22. Koike M et al. *Rev. Sci. Instrum.* **74** 1156 (2003)
23. Dinh T H et al. *Rev. Sci. Instrum.* **87** 123106 (2016)
24. Terauchi M et al. *Microsc. Microanal.* **20** 692 (2014)
25. Terauchi M et al. *J. Electron Microsc.* **59** (4) 251 (2010)
26. Imazono T et al. *Appl. Opt.* **51** 2351 (2012)
27. JEOL Ltd. Soft X-ray Emission Spectrometer (SXES), https://www.jeol.co.jp/en/products/detail/SXES.html
28. Beiersdorfer P et al. *Rev. Sci. Instrum.* **75** 3723 (2004)
29. Dunn J et al. *Rev. Sci. Instrum.* **79** 10E314 (2008)
30. Hettrick Scientific, http://hettrickscientific.com/
31. Koch J A et al. *Phys. Rev. Lett.* **68** 3291 (1992)
32. Underwood J H et al. *Proc. SPIE* **3150** 40 (1997)
33. Wang J-J et al. *Chinese Phys. C* **39** 048001 (2015)
34. Du L et al. *Nucl. Instrum. Meth. Phys. Res. A* **877** 65 (2018)
35. Miyake A et al. *Proc. SPIE* **5037** 647 (2003)
36. Fuchs O et al. *Rev. Sci. Instrum.* **80** 063103 (2009)
37. Chuang Y-D et al. *Rev. Sci. Instrum.* **88** 013110 (2017)
38. Warwick T et al. *J. Synchrotron Rad.* **21** 736 (2014)
39. Dvorak J et al. *Rev. Sci. Instrum.* **87** 115109 (2016)
40. Imazono T et al. *Appl. Opt.* **57** 7770 (2018)
41. Kolachevsky N N, Pirozhkov A S, Ragozin E N *Quantum Electron.* **30** 428 (2000); *Kvantovaya Elektron.* **30** 428 (2000)
42. Pirozhkov A S, Ragozin E N *Phys. Usp.* **58** 1095 (2015); *Usp. Fiz. Nauk* **185** 1203 (2015)
43. Ziegler E et al. *Proc. SPIE* **3737** 386 (1999)
44. Rife J C et al. *Phys. Scr.* **41** 418 (1990)
45. Barbee T W, Bixler J V, Dietrich D D *Phys. Scr.* **41** 740 (1990)
46. Senf F et al. *Opt. Express* **24** 13220 (2016)
47. Sokolov A et al. "High efficiency multilayer coated blazed grating for tender X-rays", in *Physics of X-Ray and Neutron Multilayer Structures Workshop 2016*: *PXRNMS Workshop, Enschede, Netherlands, 10 November 2016*; https://www.utwente.nl/en/tnw/xuv/workshops/archive/pxrnm-workshop-2016/oral-presentations/sokolov-pxrnms-2016-high-efficiency-multilayer-coated-blazed-grating-for-tender-x-rays.pdf
48. Hettrick M C, Bowyer S *Appl. Opt.* **22** 3921 (1983)
49. Hettrick M C et al. *Appl. Opt.* **24** 1737 (1985)
50. Bowyer S et al. *Astrophys. J. Suppl.* **102** 129 (1996)
51. Sirk M M et al. *Astrophys. J. Suppl.* **110** 347 (1997)
52. Craig N et al. *Astrophys. J. Suppl.* **113** 131 (1997)
53. The Space Telescope Science Institute (STScI). EUVE All-Sky Survey Results, https://archive.stsci.edu/euve/allsky/results.html
54. Poletto L, Tondello G *Appl. Opt.* **40** 2778 (2001)
55. Frassetto F et al. *Opt. Express* **21** 18290 (2013)
56. Firsov A et al. *J. Phys. Conf. Ser.* **425** 152013 (2013)
57. Mitzner R et al. *J. Phys. Chem. Lett.* **4** 3641 (2013)
58. Erko A et al. *Opt. Express* **22** 16897 (2014)
59. Mantouvalou I et al. *Appl. Phys. Lett.* **108** 201106 (2016)
60. Yin Z et al. *Opt. Lett.* **43** 4390 (2018)
61. Kando M et al. *Phys. Rev. Lett.* **103** 235003 (2009)
62. Vishnyakov E A, Shatokhin A N, Ragozin E N *Quantum Electron.* **45** 371 (2015); *Kvantovaya Elektron.* **45** 371 (2015)

63. Vishnyakov E A et al. *Quantum Electron.* **47** 54 (2017); *Kvantovaya Elektron.* **47** 54 (2017)
64. Shatokhin A N et al. *Opt. Express* **26** 19009 (2018)
65. Vishnyakov E A et al. *Quantum Electron.* **48** 916 (2018); *Kvantovaya Elektron.* **48** 916 (2018)
66. Levashov V E, Mednikov K N, Pirozhkov A S, Ragozin E N *Radiat. Phys. Chem.* **75** 1819 (2006)
67. Ragozin E N et al. *Proc. SPIE* **4782** 176 (2002)
68. Kolesnikov A O, Vishnyakov E A, Ragozin E N, Shatokhin A N *Quantum Electron.* **50** 967 (2020); *Kvantovaya Elektron.* **50** 967 (2020)
69. Shatokhin A N, Vishnyakov E A, Kolesnikov A O, Ragozin E N *Quantum Electron.* **49** 779 (2019); *Kvantovaya Elektron.* **49** 779 (2019)
70. Kolesnikov A O, Vishnyakov E A, Shatokhin A N, Ragozin E N *Quantum Electron.* **49** 1054 (2019); *Kvantovaya Elektron.* **49** 1054 (2019)
71. Harada T et al. *J. Jpn. Soc. Precision Eng.* **42** 888 (1976)
72. Hitachi High-Tech America, Inc. Diffraction Gratings, http://www.hitachi-hightech.com/us/product_detail/?pn = ana-grating
73. Namioka T, Koike M *Appl. Opt.* **34** 2180 (1995)
74. Koike M et al. *Proc. SPIE* **4146** 163 (2000)
75. Shimadzu. Diffraction Gratings. Laminar-type Replica Diffraction Gratings for Soft X-ray Region, https://www.shimadzu.com/opt/products/dif/o-k25cur0000006zd0.html
76. Lin D et al. *J. Synchrotron Rad.* **26** 1782 (2019)